



UNIVERSIDADE D  
COIMBRA

Oday Allan

**THE INFLUENCE OF LOW-FRICTION TMD  
COATINGS ON THE TRIBOLOGICAL  
PERFORMANCE OF SURFACE TEXTURED  
STEELS**

VOLUME 1

**Dissertação no âmbito do Mestrado Conjunto Europeu em tribologia de Superfícies e interfaces orientada pelos Professor Albano Cavaleiro e apresentada ao Departamento de Engenharia Mecânica da Faculdade de Ciências e Tecnologia da Universidade de Coimbra.**

Julho de 2021

1 2



9 0

FACULDADE DE  
CIÊNCIAS E TECNOLOGIA  
UNIVERSIDADE DE  
COIMBRA

# The Influence of Low-Friction TMD coatings on The Tribological Performance of Surface Textured Steels

Submitted in Partial Fulfilment of the Requirements for the Degree of European  
Joint European Master in Tribology of Surfaces and Interfaces.

## A influência de revestimentos TMD de baixo atrito no desempenho tribológico de aços texturizados

Author

**Oday Allan**

Advisors

**Prof. Albano Cavaleiro**

**Eng. Fátima Rosa**

Jury

**President**      **Professor Bruno Trinadade**  
Professor at University of Coimbra

**Vowel**        **Professor Sofia Ramos**  
Professor at University of Coimbra

**Advisor**      **Professor Albano Cavaleiro**  
Professor at University of Coimbra

1 2



9 0

UNIVERSIDADE DE  
COIMBRA



**Coimbra, Julho de 2021**

## **ACKNOWLEDGEMENTS**

I would like to recognize all the great support of my supervisor Prof. Albano Cavaleiro, for always guiding me, and for contributing with new ideas to overcome the inherent obstacles of scientific investigation. Additionally, I would also like to acknowledge the help and suggestions provided by Dr. Todor Vuchkov, Dr. Pooja Sharma, Eng. Fátima Rosa, the technical staff of the Institute Pedro Nunes, who contributed to this research with their experience in the experimental field.

I would also like to express my sincere appreciation to all the knowledgeable Professors, lecturers, and Colleagues from the University of Leeds, Ljubljana, and Coimbra for all the guidance and support that I received in these two years, helping with the completion of this master's program. Many thanks to TRIBOS Consortium, who selected me for this prestigious program.

Finally, I thank my family for continually motivating and supporting me throughout this journey. Above all, to the great Almighty God, who is the author of all knowledge and pearls of wisdom.

## Abstract

The goal of this research study was to investigate the effects of applying TMD coatings on the tribological performance of surface textured steel with a horizontal and vertical lines geometry giving the shape of squared grooves. Tribological experiments under both unidirectional and reciprocating sliding were done for both dry and lubricated contact. The effects of varying sliding speed, lubricant viscosity, and counter-body shape on the coefficient of friction were studied. Grooved patterns were produced on steel samples by laser surface texturing (LST). In the scope of this study, coated textured specimens showed little to no improvement in relation to smooth-coated specimens for both dry and lubricated contact. When studying uncoated specimens, the biggest improvement in terms of COF reduction for textured specimens was observed in the boundary lubrication regime at low sliding speeds, as well as in dry contact experiments.

**Keywords** Surface texturing, Grooves, Pin-on-disk, Stribeck curves, Lubrication regimes, TMD coatings.

## Resumo

O objetivo deste estudo foi investigar os efeitos da aplicação de revestimentos do tipo TMD (dicalcogenetos de metais de transição) no desempenho tribológico de aços texturizados com laser, com uma geometria de linhas cruzadas horizontais e verticais, dando origem a um formato com quadrados na superfície. Foram realizados testes tribológicos com deslizamento alternativo ou unidirecional em ambos os contatos sem e com lubrificação. Foram também estudados os efeitos da variação da velocidade de deslizamento, da viscosidade do lubrificante e da forma do contra corpo no coeficiente de atrito. Os sulcos da textura foram produzidos nas amostras de aço por texturização superficial com laser (LST). Foi possível concluir que as amostras revestidas após texturização não mostraram melhorias importantes em relação às amostras não-texturizadas revestidas em ambos os casos de contato com e sem lubrificação. No que respeita às amostras não revestidas, a maior melhoria nas amostras texturizadas, em termos de redução do coeficiente de atrito, foi observada no regime de lubrificação limite para baixas velocidades de deslizamento, assim como nos testes em contato não lubrificado.

**Keywords** Texturização de superfície, Sulcos, Pino-disco, Curvas Stribeck, Regimes de lubrificação, Revestimentos TMD.

# Table of Contents

ACRONYMS/ ABBREVIATIONS.....	vi
1. Introduction .....	1
1.1 Motivation.....	1
1.2 Organization of the Thesis.....	2
2. State of the Art .....	2
2.1 Surface Texturing.....	4
2.2 Surface Texturing Techniques .....	5
2.3 Surface Texturing Parameters .....	6
2.3.1 Effects of Textures Size, Shape, and Orientation.....	7
2.3.2 Texture Area Density.....	9
2.4 Grooved Surface Textures.....	9
2.5 Transition metal dichalcogenides (TMDs).....	11
2.5.1 Physical Vapor Deposition.....	12
2.5.2 W-S-C Coatings.....	13
2.5.3 Combining Surface Texturing with W-S-C Coating.....	13
2.6 Effect of Surface Textures on Different Lubrication Regime.....	17
2.7 Research Gaps .....	20
2.7.1 Thesis Objectives .....	20
3. Experimental Details.....	21
3.1 Specimen Details .....	21
3.1.2 Surface Texturing.....	21
3.1.3 Surface Coating.....	22
3.2 Characterization Techniques .....	24
3.2.1 3D Optical Microscopy .....	24
3.2.2 Scanning Electron Microscopy (SEM).....	24
3.3 Characterization of Samples Surfaces.....	25
3.3.1 Geometrical Characterization of Specimens .....	25
3.3.2 Morphological Analysis of Surfaces .....	27
3.4 Tribological Experiments.....	29
3.4.1 Pin-on-disk.....	29
3.5 Reciprocating Lubricated Pin-on-disk .....	32
3.5.1 Spherical Pin .....	34
3.5.2 Flat-on-Flat .....	34
3.6 Reciprocating Dry Contact.....	34

3.7 Unidirectional Lubricated Experiments.....	34
4. Results and Discussions .....	35
4.1 Preliminary Results .....	35
4.2 Reciprocating Lubricated Pin-on-disk (ball).....	37
4.3 Reciprocating Lubricated Flat-on-flat .....	38
4.4 Unidirectional Lubricated Tests .....	39
5. Conclusions .....	43
5.1 Conclusions.....	43
5.2 Final Discussion and Recommendations.....	44
Bibliography .....	45

## ACRONYMS/ ABBREVIATIONS

Abbreviation	Description
3D	Three-dimensional
BL	Boundary Lubrication
COF	Coefficient Of Friction
DLIP	Direct Laser Interference Patterning
ECMM	Electrochemical micromachining
ED	Electric discharge
EDS	Energy Dispersive Spectroscopy
HD	Hydrodynamic Lubrication
IPN	Instituto Pedro Nunes
LST	Laster Surface Texturing
MEMS	Micro-electrical mechanical systems
ML	Mixed Lubrication
Nd:YAG	Neodymium-Doped Yttrium Aluminum Garnet
PVD	Physical Vapor Deposition
$R_a$	Arithmetic surface roughness
$R_q$	Root mean square of the surface roughness
SAE	Society of Automotive Engineering
SC	Smooth and Coated
SEM	Scanning Electron Microscopy
SU	Smooth and Uncoated
TC	Textured and Coated
TMD	Transition Metal Dichalcogenides
TU	Textured And Uncoated
UM	University of Minho
W-S-C	Tungsten-Sulfur-Carbon
XRD	X-Ray Diffraction
ZDDPs	Zinc-diorganodithio-phosphates

# 1. Introduction

The present research work entitled "The influence of low-friction TMD coatings on the tribological performance of surface textured steels" envisages the study on the feasibility of self-adaptive transition metal dichalcogenide (TMD) coatings on laser textured steel. This chapter emphasizes on building the relevance of the role of transition metal dichalcogenides (TMD) coatings on textured surfaces in the modification of friction and wear for tribological contacts.

Most of the mechanical applications suffer from fuel loss due to high friction. Friction is one of the biggest contributors to fuel loss; in automobile industry alone, friction losses contribute to approximately 40% of the total energy used. Although automobiles have hundreds of parts in contact, the primary sources of frictional losses are the piston, piston-ring, and valve train systems that account for approximately 60% of the total energy used in an automobile [1]. The development of automobile industry is governed by two major factors, customer satisfaction, and environmental protection. Therefore, improving fuel economy is a crucial and essential element for the improvement of these two factors [1].

Automobiles rely heavily on the use of lubricants to reduce friction and improve fuel economy. Since the 1940s, ZDDPs (zinc-diorganodithio-phosphates) have been widely used as a lubricant additive, providing both antioxidant and anti-wear/extreme-pressure activity [2]. ZDDPs have the tendency to decompose and form volatile and toxic phosphorous species, which affect catalytic converters. The use of ZDDPs have been heavily restricted to reduce pollution, filter clogging, and waste disposal. Therefore, the development of novel technologies to reduce friction is crucial [3]. These technologies will be highly beneficial and applicable for different mechanical devices.

## 1.1 Motivation

Both TMD coatings and surface texturing have proven to improve tribological behavior under specific conditions separately. In this project, a novel approach of applying self-adaptive transition metal dichalcogenide (TMD) coatings on laser textured steel (perpendicular lines grooves) will be explored to reduce friction under different lubrication conditions.

## 1.2 Organization of the Thesis

This thesis entitled "The influence of low-friction TMD coatings on the tribological performance of surface textured steels" has been divided into six chapters. Chapter 1 establishes the link between surface texturing, TMD coatings, and friction & wear reduction, and it also discusses this project's contributions to the field. Chapter 2 covers the concise review of the literature on the effect of surface texturing (different geometrical shapes and densities) on friction and wear. Emphasis has been given on elaboration of the mechanisms involved in friction and wear of textured surfaces. Furthermore, it describes the effect of W-S-C coating on the tribological behavior of contacts. At last, it talks about the objectives of the thesis and the research gaps. Chapter 3 covers a detailed description of the experimental methods used for the present investigation is furnished. This chapter also includes a description of the raw materials used for the current research, preparation of the samples in terms of surface texturing and coating, the details of various experimental techniques used, experimental conditions employed, and the parameters fixed for each individual experimentation. Chapter 4 discusses the results of preliminary experiments that were discarded due to repeatability issues, it also includes the results and discussions of completed tribological experiments. Chapter 5 includes final conclusions of the thesis, as well as final discussion and recommendations for future work.

## 2. State of the Art

This project investigates the effects of TMD coatings on friction and wear for surface textured steels. This chapter covers previous research related to surface texturing and TMD coatings. It discusses the effect of surface texturing on friction and wear under different lubrication regimes. The use of different surface texturing parameters is studied. It also investigates the mechanisms involved in friction and wear of textured surfaces. At last, it studies the effect of W-S-C coating on the tribological behavior of contacts.

Tribologists have been trying, over the years, to minimize friction and wear for many applications. Surface texturing has been mainly used in the production of automotive components, tools, punches of metal forming processes, and micro-electrical mechanical systems (MEMS). The following is a brief description of the use of texturing in some of the industries mentioned.

In the automobile industry, Hamilton et al. [4] used micro asperities as hydrodynamic bearings in parallel sliding applications, such as face seals and rotary shafts. Anno et al. [5] proved that micro texturing only one of the parallel surfaces of the rotary shaft face seals increased the load-carrying capacity. Cylinder bores of internal combustion engines were textured by Willis [6], while Wakuda et al. [7] studied the effect of textured surface dimples on nitride silicon ceramic plates, which are used in automobile engines as a structural element. The latter investigated different texture dimple densities but kept the depth constant at five  $\mu\text{m}$ . Best results attained 20% friction reduction under boundary and mixed lubrication using pin-on-disk set-up, while using 5 to 20% textures density.

Wang et al. [8] found that texturing SiC thrust bearings sliding in water doubled their load-carrying capacity in the regime in-between hydrodynamic and mixed lubrication.

Etsion et al. [9] and Yu et al. [10] showed a 30% reduction in coefficient of friction (COF), by laser texturing mechanical face seal rings. Friction losses due to cylinder liner-piston ring system are estimated to be 30% of total engine friction loss [11].

In MEMS applications, surface texturing is one of the few methods to control friction and adhesion, because lubrication is not an option. Baumgart et al. [12] created round dome-like protrusions on the inner diameter of the hard disk, successfully reducing stiction at start-up

In metal forming industry, such as deep drawing process is shown in Figure 1 [13]. Wiklund et al. [60] showed a linear relationship between the coefficient of friction and surface roughness of the blank. Geiger et al. [14], [15] examined the relevance of laser texturing on

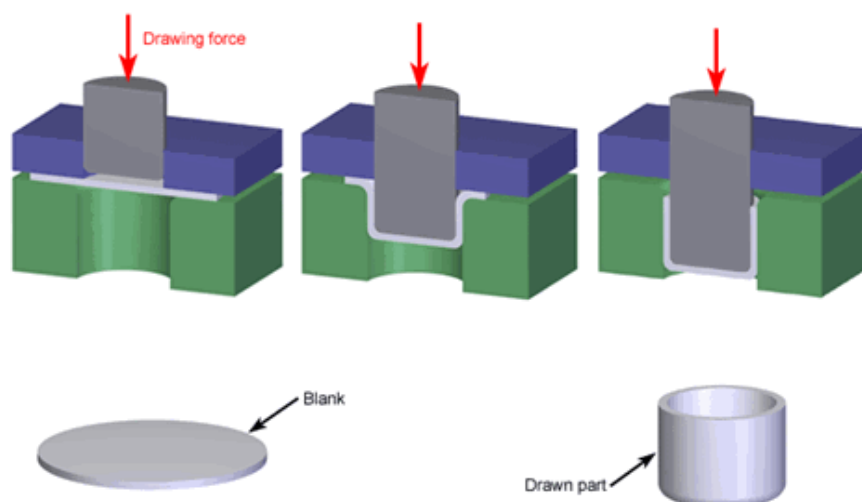


Figure 1: Deep drawing process [13].

the tool and its effect on micro-lubrication. They concluded that the shape and depth of the textures had an effect on friction in strip drawing.

## 2.1 Surface Texturing

Surface texturing is defined as the process of creating a specific type of pattern on the workpiece surface in order to modify its surface features. The scale of surface texturing can range from the nanoscale to the milli scale. For engineering applications, surface texturing is used to improve the performance of surfaces (e.g., wear reduction) [16].

The use of non-isotropic surfaces in engineering applications is being studied very slowly due to the fact that any texturing to the surface will increase the roughness, therefore usually increasing wear and friction [16].

Surface textures can be observed in nature. Shark's skin contains 3-D patterns to reduce drag and turbulence, which is also used in modern swimming suits. Hydro affinity can also be controlled with surface texturing. Table 1 summarizes functions and applications of surface texturing for different applications [16].

Table 1: Functions and applications of different types of textures on engineered surfaces [16]

<b>Domain</b>	<b>Functions</b>	<b>Applications</b>	<b>Types of texture</b>
<b>Biomedical</b>	Implant adhesion, friction reduction	Implants	Micro-dimples
<b>Tribology</b>	Improving lubrication, reducing friction, increasing load capacity	Piston rings, bearings	Micro-dimples, grooves
<b>Aerodynamics</b>	Drag reduction	Aircrafts	Parallel axial ribs
<b>Wetting</b>	Contact angle and surface energy	Ship hull, propeller, surgical tools	Micro-pillar array, needle array
<b>Optics</b>	Refraction, diffraction, light adsorption	Wavelength specific mirrors	Groves, micro patterns
<b>Mechanics</b>	Strength, adhesion, wear resistance	Seashell, tooth,	Natural textures

<b>Plant</b>	hydrophilicity, hydrophobicity	reduction of Natural textures contamination, windshields
--------------	-----------------------------------	--

There are multiple instances of the use of surface texturing to increase friction and traction throughout history. The Tong dynasty in China used ridged patterns on the soles of laborers' shoes working on muddy and slippery ground [5]. In modern times, tires for automobiles use different types of patterns, making driving safer under different conditions [17]. On the other hand, in the scope of surface engineering, the focus has been to achieve the lowest possible roughness (smooth surfaces) to minimize friction and wear [17].

In the past, piston ring liner of diesel engines running under high speed, load, and temperature conditions had severe scuffing and ultimately seizure and failure due to lubricant starvation, which led to the first use of surface texturing in the 1940s. Piston liners started getting manufactured with cross-hatched grooves with 60° to 70° angles to function as a local lubricant source. Modern diesel engines started using 40° to 50° horizontal crossover angles instead [18], [19], [20].

There have been a lot of successful applications of surface texturing, such as mechanical face seals with laser surface textures, to reduce friction between contacting bodies; in metal forming processes to control adhesion and heat diffusion; magnetic storage disks to control area of contact and control stiction at the interface of head/disk [21], [22], [23].

## 2.2 Surface Texturing Techniques

In the 1990s, laser (LST) and electrochemical (EC) surface texturing techniques were widely used in the production of magnetic storage devices and mechanical seals. At that time, LST texturing was progressing towards shorter pulses, providing more flexibility in terms of processed materials. LST can produce well-defined and consistent micro surface textures on both metals and non-metals. However, it is not economically feasible to use it on nanoscale though. It is also limited to macro surfaces because lasers can melt or distort micro and nano workpieces [16].

Similarly, to LST, Electric discharge (ED) is also thermal based texturing technique. However, it has the same limitations as LST, possibly causing distortion or vaporization of

nano/microstructures. Other disadvantages of using ED are the introduction of micro cracks, residual thermal stresses, and recast layer [16].

Direct Laser Interference Patterning (DLIP) allows the use of multiple laser beams to create complex surface textures in one step.

Plenty of other techniques are being developed. Choosing a surface texturing technique usually depended on dimensions, speed, and cost [24], [25].

At the beginning of the 21<sup>st</sup> century, nanotechnology was quickly developing, introducing new and relatively cheap methods of surface texturing on the nanoscale. Nano casting and lithography are not viable for large-scale production because they require multiple steps, namely, insulation, mask generation, and machining [16].

The analysis of fabricated surfaces dramatically improved with the introduction of white light interferometric surface analysis, allowing more accurate characterization of textures, hastening the development of texturing techniques [26].

Both electron beam machining (EBM) and focused ion beam milling (FIBM) are very good for texturing in the micro and nanoscale, but they require a lot of time to texture bigger samples [16].

Chemical texturing can be used for bigger samples (millimeter scale), but it is very difficult to control the variables and require vast knowledge in chemistry because each element requires a specific etchant [16].

Electrochemical (EC) processes, such as jet electrochemical micromachining (ECMM) and through-mask electrochemical micromachining (TMEMM), are promising techniques; in order to reproduce accurate textures, a mask needs to be designed and fabricated using a different method, such as lithography or laser machining. Once fabricated, the mask can be reused to create quickly create textured surfaces [16].

### 2.3 Surface Texturing Parameters

There are plenty of parameters that can be controlled while producing surface texturing, such as shape, dimensions, direction, and spacing of textures. Testing conditions (e.g., type of test, speed, lubrication regime, etc.) also play a huge role in choosing the best parameters. As a result of the different texturing parameters and of plenty of testing conditions available, contradicting results are found among the literature [26].

Surface texturing could be positive or negative. Positive texturing is protruding from the surface, which is useful in electronics, MEMS, and magnetic disks applications. Negative surface texturing is inner surface textures, can be as grooves or dimples or any other shapes. It is useful in automotive applications and cutting tools. Negative texturing is addressed in this thesis.

### 2.3.1 Effects of Textures Size, Shape, and Orientation

The influence of geometrical shape and orientation on the coefficient of friction was studied by Hsu [27], with speed ranging from 0.023 to 0.23 m/s and pressures ranging from 0.03 to 1.1 MPa. A flat-on-disk set-up was used, with steel-on-steel contact.

As shown in Figure 2, Hsu concluded that the geometrical shape of textures could have a huge effect on COF. Overall, elliptical shapes and perpendicular contact direction achieved the best COF [27]. However, contradicting this result, Siripuram et al. [28] concluded that surface textures shapes had no effect on COF, although they did not test elliptical shapes.

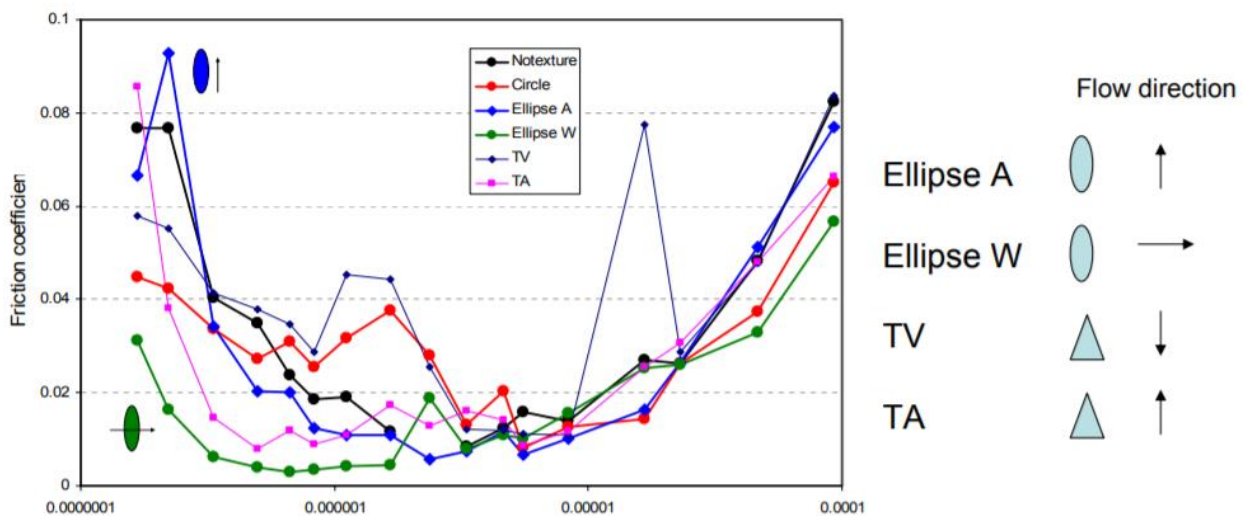


Figure 2: Stribeck curve for different textures shapes and orientations as studied by Hsu using Flat-on-disk set-up, with steel-on-steel contact [27]

Pettersson et al. [29] investigated friction and wear properties of boundary lubricated textured surfaces. Square depressions and parallel grooves of different widths were produced using lithography and etching. Silicon wafers were used, and PVD coated with a thin layer of diamond-like carbon (DLC) to maintain original surface textures. Reciprocating ball-on-flat set-up was used under starved or lubricated boundary conditions.

Figure 3 summarizes the performance of different surface textures shapes and orientations according to the research conducted by Pettersson et al. [29]. The circles represent elastic contact area calculated using the Hertz model with a load of 5N (680MPa) (steel ball against silicon wafers). The influence of the DLC coating is neglected. The diameter of the contact area is estimated to be 120  $\mu\text{m}$ . Tested textures had three different widths: 5 (3.5  $\mu\text{m}$  depth), 20 and 50  $\mu\text{m}$  (5  $\mu\text{m}$  depth).

According to this study [29], under starved lubrication conditions, textures with small grooves/squares with perpendicular orientation achieved a much lower coefficient of friction values than non-textured surfaces. However, for lubricated boundary conditions, with ample oil supply, this study concluded that texturing had no effect on COF, resulting in a consistent value of 0.08 to 0.1, whereas successful textured starved surfaces had a COF value of 0.05.

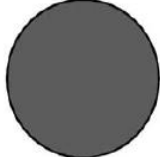
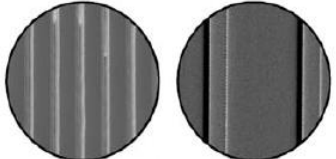
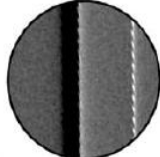
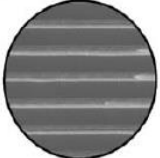
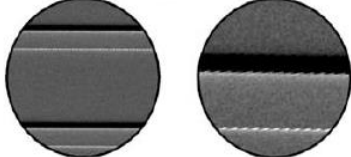
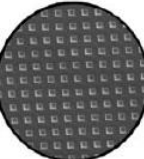
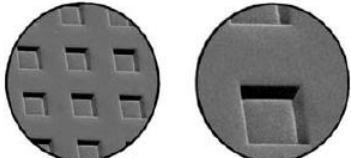
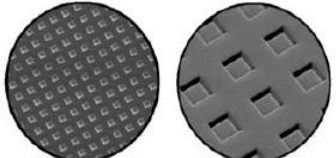
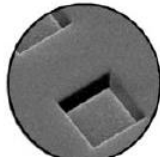
Surface texture (orientation)	Low friction and no measurable wear	High friction and severe wear
Sliding direction of the ball 		
Flat reference		
Grooves (perpendicular to sliding direction)		
Grooves (along sliding direction)		
Square depressions (along sliding direction)		
Square depressions (30° from sliding direction)		

Figure 3: Summary of textured surfaces performance. Circles show the elastic contact area calculated by Hertzian equations with a load of 5 N. coating influence on calculated contact area is neglected [29]

### 2.3.2 Texture Area Density

According to the literature, surface texture density can be defined as a function of both the width/diameter and the spacing of textures. However, there is not a single value that suits all applications and conditions. Rashwan [30] suggested that minimum COF is attained when surface texture density is between 25 to 50%. Figure 4 shows Rashwan's results for three different depths, under dry contact conditions for surface-textured specimens (dimples),  $D$  is in  $\mu\text{m}$  [30].

The behavior of COF seen in Figure 4 can be explained by the combination of adhesive and mechanical deformations due to stresses. At textures density of more than 50%, adhesive forces are small, but mechanical stresses are high, due to smaller contact areas. At low surface texture density, adhesive forces are high, and mechanical stresses are relatively low (low plastic flow and smaller plowing) [30].

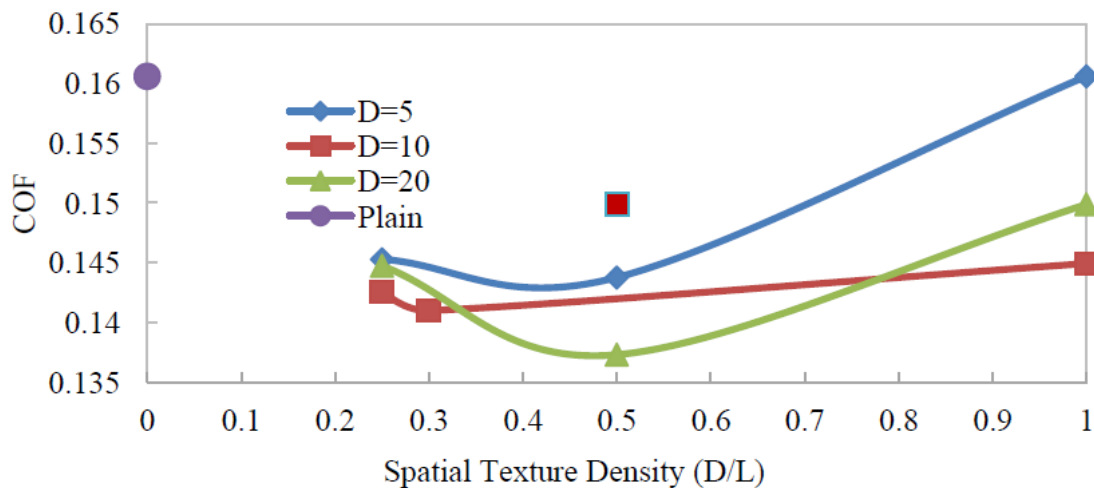


Figure 4: Effect of surface texture density on COF for dry contact.  $D$  is dimple depth in  $\mu\text{m}$  [30]

### 2.4 Grooved Surface Textures

Vilhena et al. [31] studied the effect of rhombic grooved surfaces by electrical discharge machining (EDM) under different lubrication regimes. This study focused on the effect of textures density on the coefficient of friction by varying sliding speed and lubricant viscosity. Rhombic geometry is shown in Figure 5 [31].

Steel disk specimens used were prepared from AISI M2, quenched, and tempered to 710HV by machining and mirror polished to surface roughness of  $R_a = 0.01\mu\text{m}$ . The specimens were analyzed using a white light 3D scanning microscope and summarized in Table 2 [31].

Samples were tested using a block-on-ring set-up under unidirectional sliding motion. Counter body (ring) was made of 3415 AISI steel with a hardness of 237 HV, positioned 90° to the ring's rotational axis. The contact was flooded across the experiments, using three different lubricants were used, ISO VG 46, 150, and 320 [31].

Table 2: Measured dimensions for textured specimens [31]

<i>Surface Texture Density</i>	<i>Low</i>	<i>Medium</i>	<i>High</i>
<i>Distance between grooves, <math>\mu\text{m}</math></i>	1294	603	390
<i>Groove width, <math>\mu\text{m}</math></i>	142	149	159
<i>Groove depth, <math>\mu\text{m}</math></i>	16.3	15.8	17.8
<i>Rhomb width, <math>\mu\text{m}</math></i>	1331	524	267
<i>Area density %</i>	21	44	65

Specimens were polished again after texturing to remove grinding marks and achieve similar roughness to smooth samples. Six different speeds were tested under a constant load of 25N (0.03 Hertzian contact pressure). Tested speeds were: 0.03, 0.1, 0.25, 0.5, 1.0, and 1.27 m/s, and number of turns were set to 100, 250, 500, 1000, 1000, and 1000 [31].

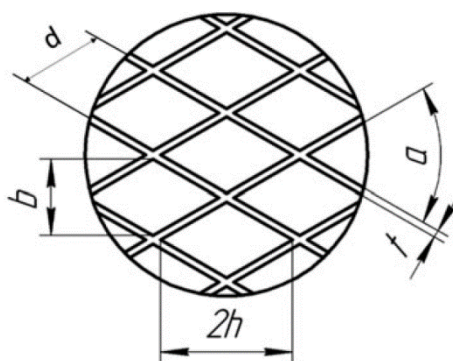


Figure 5: Rhombic shape parameters [31]

It can be concluded from this study, as Figure 6 and Figure 7 illustrate, that surface texturing reduced COF when using high viscosity or low viscosity oil for high speeds (corresponding to the hydrodynamic regime). For medium viscosity oil, friction reduction can also be observed in mixed lubrication regime [31].

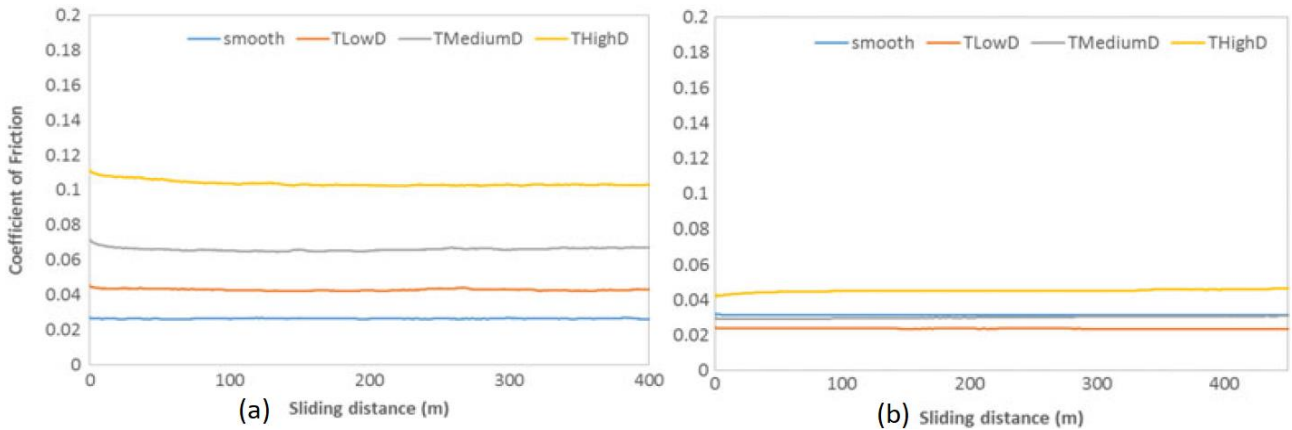


Figure 6: Friction curve for textured and untextured surfaces, both using ISO VG 46, but with two different sliding speeds of: a) 0.5m/s – boundary/mixed regime, b) 1.27m/s hydrodynamic regime [31]

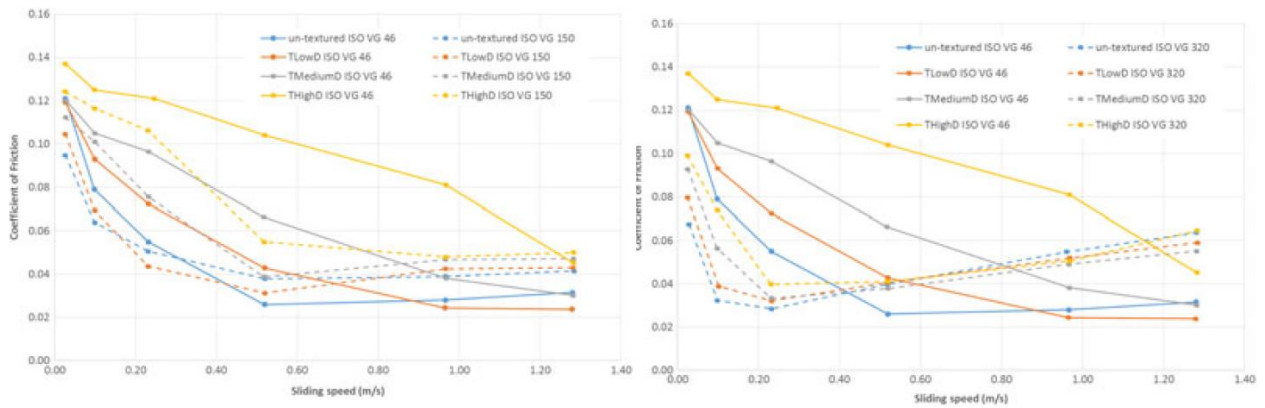


Figure 7: Friction curve for textured and untextured surfaces, plotted against sliding speed comparing 3 different lubricants [31]

## 2.5 Transition metal dichalcogenides (TMDs)

Transition metal dichalcogenides (TMDs), such as molybdenum and tungsten disulfides and diselenides, exist in two crystal structures, rhombohedral and hexagonal [32]. In the scope of this project, hexagonal form is more interesting, given its effectiveness in low friction applications.

The hexagonal crystal structure consists of a six-fold symmetrical lamellar structure. Each chalcogenide atom (sulfur or selenide) is equally spaced from three metal atoms (molybdenum or tungsten), and each metal atom is equidistant from the six chalcogenide atoms. Slip occurs between these atoms due to the large spacing between metals and chalcogenides. Weak van der Waals forces also promote easy inter and intra-crystalline slip.

TMDs have similar interfacial and inter-crystalline friction, as well as high resistance to asperity penetration under high pressures and anisotropic properties due to their strong covalent bonding and layered nature, respectively [33].

TMDs have weak inter-lamellar bonding, causing low friction (because layers can be sheared easily). However, the presence of contaminants increases these lamellar interactions, and therefore, increases friction. For this reason, TMDs have high friction values in humid or contaminated contact. Other known layered materials, such as graphite or mica, have covalent bonding. These materials depend on contaminants to reduce their bond energies, which is why they reduce friction in humid environments (water vapor) [34].

TMDs are used as thin films, oil additives, or solid lubricants. Thin films are mostly prepared using magnetron sputtering. The most widely used member of TMDs is molybdenum disulfide ( $\text{MoS}_2$ ), and it was highly investigated in the 1990s. However, back then, deposition on steel substrate was limited, and only low adhesion was achieved, causing quick wear of coatings, especially in the presence of humidity. As a result, they are considered unstable for tribological testing under high pressures and humid environments. Different TMDs have similar properties. However, diselenides have better water resistance properties compared to sulfides [35].

Still, TMDs have their drawbacks, such as low adhesion to the substrate, very low load-bearing capacity, and increased friction in the presence of humidity. The most commonly used method used to overcome these drawbacks is doping with high-strength material, usually titanium. [36] [37].

### 2.5.1 Physical Vapor Deposition

Sputtering was first performed back in the 1850s but remained a scientific curiosity until the 1940s. Sputtering is the technique by which atoms or molecules of a material are ejected from a target due to the bombardment of high-energy particles. Nonetheless, sputtering has very low deposition rates and a high cost. In the mid-1970s, a magnetically improved modification of sputtering, known as magnetron sputtering, emerged [38].

Magnetron sputtering is a high-rate vacuum coating technique for depositing metals, alloys, and compounds onto a wide range of materials. Coatings have thicknesses up to a few microns. There are many advantages of magnetron sputtering such as High deposition rate, the possibility of automating the process, the ability to sputter any metal, alloy, or compound,

high purity, coatings have strong adhesion to the substrate, good step coverage, ability to coat heat-sensitive materials, and uniformity even on complicated shapes [38].

Power is supplied to a magnetron, applying a negative voltage of typically – 300 V to the target. This negative voltage attracts positive ions to the target surface, inducing, at the same time, large kinetic energy. Energy transfer occurs when a positive ion hits an atom at the surface of the target. If the energy transferred to the atom is larger than the binding energy, primary recoil atoms can be generated. These atoms can collide with other atoms, causing a collision cascade. Sputtering happens if the energy transferred in a direction normal to the surface is bigger than three times the surface binding energy (approximately equal to the heat of sublimation) [38].

### 2.5.2 W-S-C Coatings

Voevodin et al. [39] and Nossa and Cavaleiro [40] alloyed WS<sub>2</sub> with carbon, preparing nanocomposite coatings by combining the low friction properties of WS<sub>2</sub> and the hardness of WC embedded in an amorphous carbon matrix (carbon doping). The idea behind this coating is to combine the tribological properties of DLC films in the presence of moisture (humid air) with the low frictional properties of WS<sub>2</sub> in dry air. The hardness of the coating was measured to be around 10GPa, and it also showed extremely good tribological properties in dry nitrogen environment. In the presence of humidity, the carbon matrix protected the WS<sub>2</sub> phase, increasing the endurance of the coating. However, high friction values were recorded in humid air. Alloying W-S-C with different metals could highly improve mechanical properties and adhesion of coatings to substrates; it is also possible to modify the microstructure of the coating by controlling metal content [33].

### 2.5.3 Combining Surface Texturing with W-S-C Coating

Meng et al. [41] performed tribological experiments on cemented carbides, the samples were textured and W-S-C coated. The following section shows the research details and findings.

Micro-grooves were formed on the cemented carbide surface by Nd:YAG laser. W-S-C film was deposited using physical vapor deposition (PVD), using the parameters shown in Table 3. Ball-on-disk experiments were used to study the tribological behavior. The substrate used in this research was WC+ 8 wt.% Co cemented carbide. The counter bodies were AISI 316 austenitic steel balls with 9.525mm diameter. Substrate surfaces were polished to a roughness R<sub>a</sub> less than 0.05μm, and the balls had a roughness R<sub>a</sub> of 0.1μm. [41]

A laser with 1064nm wavelength and a pulse duration of 134ns with a frequency of 30KHz was used to create the surface grooves on the cemented carbide samples. Grooves density was calculated as the width of a single groove divided by the distance between two adjacent grooves. Deburring was used after texturing to remove the bulges around the grooves. [41]

A thin Zr interlayer was deposited at the beginning to increase adhesion between the coating and the substrate. PVD was used afterward to deposit W-S-C on the surface. Figure 8 shows a SEM micrograph of surfaces before and after deposition [41].

Table 3: Texturing parameters for W-S-C [41]

Parameters	
Base pressure (Pa)	$6 \times 10^{-3}$
Working pressure (Pa)	0.6
W-S-C composite sputtering target current (A)	1.1
Deposition temperature (°C)	200
Bias voltage (V)	-80
Deposition time (min)	240

Dry contact experiments were performed using a ball-on-disk tribometer, it was used to measure friction and ambient conditions. The balls were on top, pressed against the sample in a reciprocating motion perpendicular to the direction of the grooves. The sample had dimensions of (16x16x4.5 mm). While the normal load used was 20N, speed was 10mm/s, and total run time was 3600s. Scanning electron microscopy (SEM) and energy dispersive spectroscopy (EDS) were used to analyze samples before and after the tests [41].

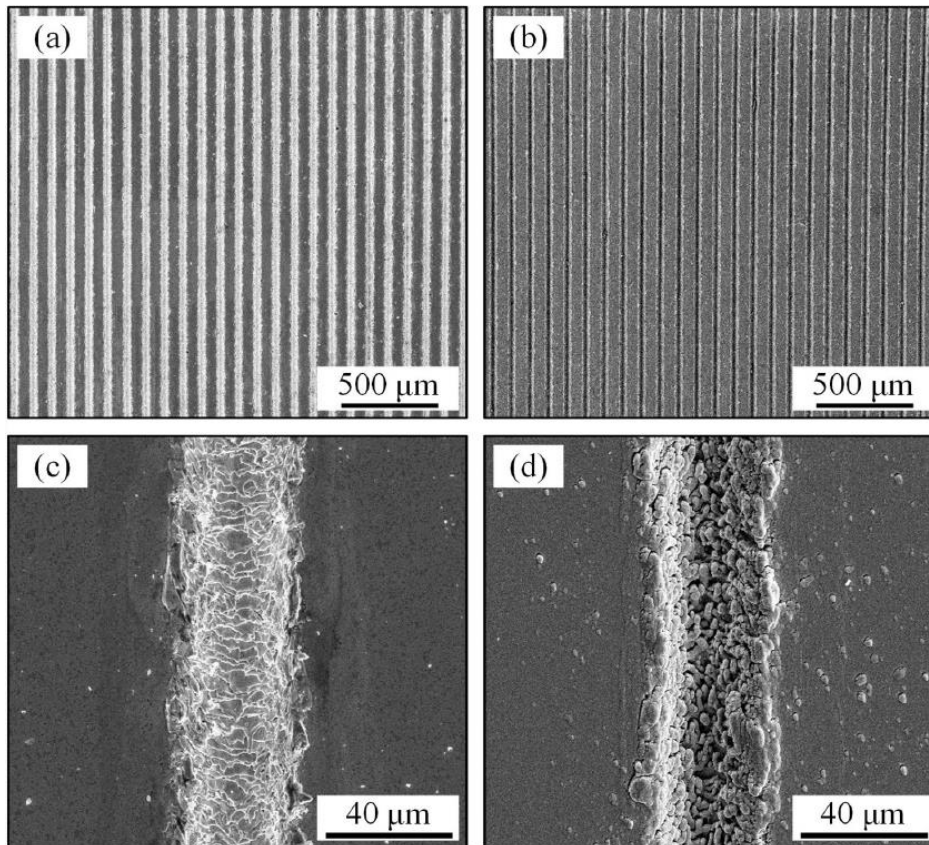


Figure 8: SEM micrograph of (a) before deposition, (b) after W-S-C deposition, (c) and (d) are zoomed graphs of (a) and (b) [41]

Coefficient of friction values for smooth specimens were initially lower than those for grooved samples, however, as friction stabilized, grooved samples attained lower COF as can be observed from Figure 9. Samples with higher grooves density also showed more stability in regard to COF values. Figure 10 (a) suggests that the use of micro-grooves is effective for dry sliding contact [41].

Nonetheless, performing the same experiments after applying W-S-C coating showed undesirable results because tests of smooth surfaces coated with W-S-C showed lower COF values than any of the textured specimens. For textured surfaces, W-S-C coatings caused a reduction in COF values for 0%, 2%, 4%, and 9% groove densities (when compared with uncoated and textured specimens) but caused a huge spike in COF values for both 18% and 35% grooves density as shown on Figure 10 (b), concluding that this type of grooves with high textures density, is not useful for dry sliding contact when W-S-C coating is used. SEM images for wear tracks showed extreme damage for coating film for textured surfaces due to plowing, indicating some serious adhesive and abrasive wear [41].

Surface texturing in dry contact enhances wear entrapment, reducing friction. For textures with high area density, W-S-C coating thickness is low inside the grooves, causing a faster film depletion and increasing, therefore, the friction. For coated specimens with low grooves density, low COF was attained by combining the low friction properties of the coating and wear entrapment of the grooves [41].

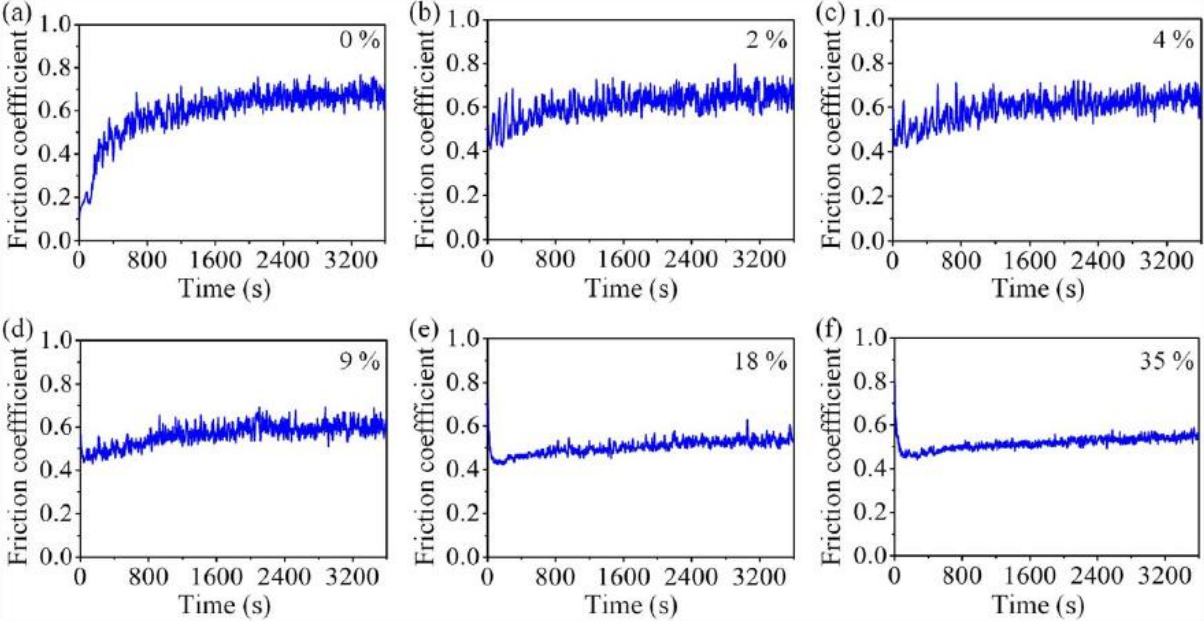


Figure 9: Friction coefficient for different textured area density (without coating) using ball-on-disk under dry lubrication [41]

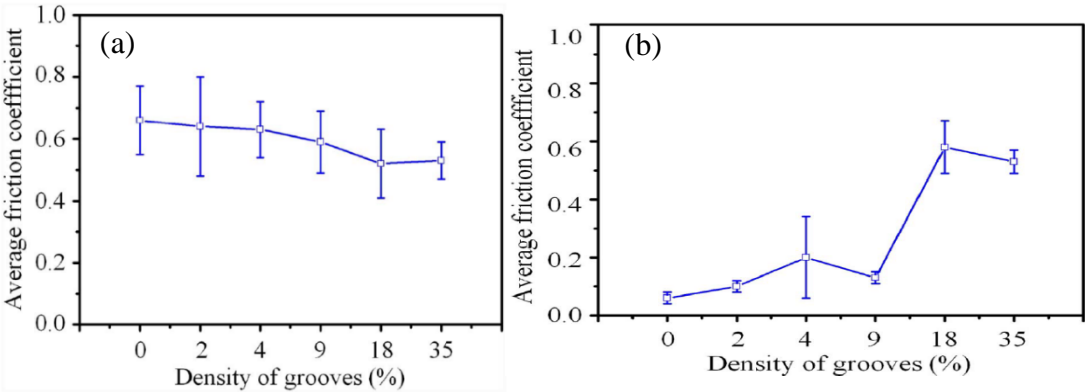


Figure 10: Steady state COF values for both uncoated (a) and coated (b) specimens, using ball-on-disk under dry lubrication [40]

## 2.6 Effect of Surface Textures on Different Lubrication Regime

Testing conditions play a big role on the effects of surface textures on both friction coefficient and wear rate. For **hydrodynamic lubrication (HD)**, a regime characterized by, high pressure, full film lubrication, and non-conformal contact, several experimental studies showed that using transverse grooves and ridges could improve mean film thickness, while using longitudinal or isotropic textures caused an undesirable effect on film thickness [42] [43] [44] [45].

Generally speaking, the literature shows undesirable effects due to surface texturing at HD contact. This occurs due to the reduction of pressure caused by texturing in HD contact, and therefore the reduction of the viscosity of the lubricant, which in turn reduces the lubricant thickness. Moreover, the generation of wear particles around the textures due to high pressures makes them unacceptable for some applications. Still, it seems to be possible to attain interesting results using textures with lower depths than 500nm [26].

**Mixed lubrication** is the most difficult regime in terms of studying textures performance; there are plenty of successful and unsuccessful cases for texturing in this regime. Kovalchenko et al. [46] showed a reduction in coefficient in friction and expanding the load-speed range for which full film lubrication occurs [47] [48]. Experiments were done on a pin-on-disk set-up with oil supplied by single drop method [26].

Borghini et al. [49] used laser surface textured specimens in the experiments, showing a 75% reduction in coefficient of friction while also showing a shift to the transition from mixed to full film lubrication at lower speeds. Braun et al. [50] performed tribological tests for conformal contact using different temperatures and different dimple sizes while keeping dimples area density at 10% and depth to diameter ratio 0.1. Their results showed an 80% friction reduction when using dimples of 200 and 40  $\mu\text{m}$  diameter at 50 °C and 100°C, respectively.

Scaraggi et al. [51] and Braun et al. [50] proposed that using micro-grooves or dimples with large diameters (300-800  $\mu\text{m}$ ) resulted in a big increase in the coefficient of friction. It is assumed that micro-grooves cannot trap lubricant efficiently due to side leakage [26]. Table 4 summarizes surface texturing effects on both full film and mixed lubrication regimes [26].

Table 4: Summary of surface texturing effects for mixed and full film lubrication [26]

	Mixed Lubrication	Full Film Lubrication (HD)	Full film lubrication (HD)
<b>Main Effects</b>	<ul style="list-style-type: none"> <li>• Entrapment of wear debris</li> <li>• secondary oil effect</li> <li>• friction reduction</li> <li>• increase of film thickness.</li> <li>• shift in Stribeck curves</li> </ul>	<ul style="list-style-type: none"> <li>• Friction reduction [52]</li> <li>• Increase of load Support.</li> <li>• Friction increase</li> </ul>	<ul style="list-style-type: none"> <li>• Increase of film thickness. [53]</li> <li>• Reduction of film thickness</li> <li>• Friction increase</li> <li>• Friction reduction [53]</li> <li>• Increase wear [53]</li> </ul>
<b>depth</b>	1 to 10 $\mu\text{m}$	6 to 10% of feature width	below 500nm
<b>width</b>	5 to 100 $\mu\text{m}$	Less than bearing width	below $\mu\text{m}$
<b>Textured Area %</b>	7 to 12%	10 to 30%	10 to 20%
<b>Shapes</b>	Pockets, Grooves (less efficient)	Pockets, Grooves (less efficient)	Pockets and Grooves
<b>Directionality</b>	Perpendicular to sliding	Perpendicular to sliding	Perpendicular to sliding
<b>Texturing Techniques</b>	LST	LST	DLIP

**Boundary lubrication** regime occurs when the contact is fully supported by asperity-to-asperity contact, friction reduction is dependent on lubricants additives (anti-wear) and surface chemistry such as ZDDP, forming a tribo-film on the surface. Since such a system is dependent on wear to reduce friction (gradual removal of tribo-film), it is, therefore, crucial to reducing roughness in order to reduce wear. Therefore, it is recommended to reduce both textures size and textured area. According to previous studies, texture area of 5% to 8% provides promising results due to their ability to retain lubricant during contact [26].

Andersson et al. [54] tested textured surfaces (circular dimples) in boundary lubrication regime, the best results were achieved when using high viscosity oil at 8% textured area. Friction reduction was not significant, but testing time dramatically increased before scuffing occurred, mainly due to trapped lubricant in the dimple and trapped wear debris.

For **dry contact** conditions, the literature shows conflicting results. Borghi et al. [49] showed a 10% decrease in COF for textured nitrided steel (dimples) due to entrapment of wear

particles. Xing et al. [55] used textured wavy patterns on Si<sub>3</sub>N<sub>4</sub>/TiC sliding against steel and achieved a COF reduction of 22.1%.

Kang et al. [56] performed experiments using smooth, nano-textured, and micro-textured dimples on aluminum surfaces. They slide the surface against half-ball shape polydimethylsiloxane rubber under different humidity conditions. The results show that both micro and nano textures caused more than two times COF increase [56]. Wang et al. [57] studied the effect of grooved microtextures on stainless steel, sliding against Al<sub>2</sub>O<sub>3</sub> ceramic balls in ball-on-flat tests under dry conditions, COF increased when grooves spacing between 15 to 35μ was used and decreased when the spacing between 50 to 300μm was used, wear rates of all textured surfaces are lower than smooth surfaces. Table 5 summarizes surface texturing effects for both dry sliding and boundary lubrication [26].

Ultimately, there are no general rules to improve friction since each contact system requires different parameters in order to improve the COF. Among these parameters, it is worth mentioning the contacting materials, coatings and, in the case of textures, its spacing, shape, and depth.

Table 5: Summary of surface texturing effects for dry sliding and boundary lubrication [26]

	<b>Dry Sliding</b>	<b>Boundary Lubrication</b>
<b>Main Effects</b>	<ul style="list-style-type: none"> <li>• Entrapment of wear debris</li> <li>• Reduction of contact area</li> <li>• Formation of tribolayers</li> <li>• Stress distribution</li> </ul>	<ul style="list-style-type: none"> <li>• Friction Increase</li> <li>• Edge of dimples</li> <li>• Increased wear</li> <li>• Dimple Worn off</li> <li>• Wear and friction reduction</li> </ul>
<b>depth</b>	below 20μm	2 to 15 μm
<b>width</b>	below 60μm	undefined
<b>Textured Area</b>	10 to 70%	undefined
<b>%</b>		
<b>Shapes</b>	Pockets and Grooves	Pockets and Grooves
<b>Directionality</b>	Non-parallel	Not Defined
<b>Texturing Techniques</b>	LST, DLIP	PCT, MECT, IPT

## 2.7 Research Gaps

Previous studies considered different surface texturing parameters under different lubrication regimes. Meng et al. [41] performed tribological experiments on W-S-C coated and line textured cemented carbides. Similarly, this project deals with W-S-C coated specimens, but the material used in this project is steel, and the textures have a shape of perpendicular lines. The main objective of this research is to study effect of texturing to on wear and friction in different lubrication regimes. The aim is to use same materials and texturing as Vilhena et al. [31] used, but the samples are W-S-C coated.

### 2.7.1 Thesis Objectives

The objective of this work is to study the effect of applying TMD coating on surface textured steels with perpendicular grooves. The experimental work involves varying the type of the counter body, the type of sliding, and the lubricant used.

### 3. Experimental Details

In this chapter, a description of the used materials for specimens used in the current research is elaborately made. As well as a detailed account of various experimental techniques used, experimental conditions employed, and parameters fixed for each individual experimentation is also provided. The methods adopted for texturing the specimens and post coating of nanocomposite layers are narrated. Details about the methodologies adopted for various characterization techniques are explained. Tribological experiments are divided into multiple sections, discussing different counter-bodies and types of motion.

#### 3.1 Specimen Details

The steel specimens of quenched and tempered (710 HV) AISI M2 steel discs were prepared by machining and polished to mirror smoothness by using diamond abrasive disk, roughness was measured using 3D optical microscopy to values of  $R_a \approx 0.01 \mu\text{m}$ . The chemical composition can be seen in Table 6. The size of each specimen is  $\varnothing 20 \times 7.8 \text{ mm}$ .

Table 6: Steel chemical composition (in weight %).

<i>Chemical Composition</i>	<i>C</i>	<i>Cr</i>	<i>Mn</i>	<i>Mo</i>	<i>V</i>	<i>Si</i>	<i>W</i>
<i>AISI M2</i>	1.00	4.15	0.3	5.0	1.95	0.3	6.25

#### 3.1.2 Surface Texturing

Polished disc specimens are textured using LST creating both vertical and horizontal lines (perpendicular to each other) on the surface. The resultant textured surface is shown in Figure 11. LST creates bulges on the edges of the textured zones, which are removed by lapping. The textured area density is calculated by dividing the surface into equal squares. The surface texturing of the specimens has been performed at the Mechanical Engineering department of the University of Minho. The laser used for texturing is SISMA Nd: YAG Laser of Class IV having Laser Power 6W@50/60kHz, wavelength 1064nm, and voltage 200-240 volts. The laser texturing has been performed at specific parameters such as the power=100% (6W), scanning Speed=150 mm/s, number of passages=20, and laser pulse frequency=50/60 kHz.

### 3.1.3 Surface Coating

Textured and smooth specimens are W-S-C coated using magnetron sputtering in a semi-industrial unit (Teer Coatings Ltd. UDP650/4, UK) with a volume of  $\sim 275 \text{ dm}^3$ . Four targets ( $340 \times 140 \times 8 \text{ mm}$ ) were mounted on the magnetrons vertically aligned on the chamber walls. Two graphite targets, one tungsten disulfide ( $\text{WS}_2$ ) and one Cr (interlayer) target were used. The coating is deposited at a target to substrate distance of 25 cm. Substrate and target configuration is shown in Figure 12 [58]. The co-deposition of TMD and C causes a formation of a nanocomposite layer over the specimens that are composed of amorphous carbon (a-C),  $\text{WS}_2$ , and tungsten carbide (WC) [58]. “A Cr interlayer with a thickness of  $\sim 300 \text{ nm}$  was deposited at the beginning, followed by a gradient Cr/WSC layer with a thickness of approximately  $100 \text{ nm}$ . The interlayer was deposited for 10min using a power density of  $3 \text{ W/cm}^2$  with a negative p-DC ( $f=250 \text{ kHz}$ , reverse time =  $1.6 \mu\text{s}$ ). The deposition of WSC coatings was performed by setting the power density of the  $\text{WS}_2$  target to  $2.1 \text{ W/cm}^2$ ”. Detailed description of how the coatings were performed can be found in the paper published by Todor et al. [58].

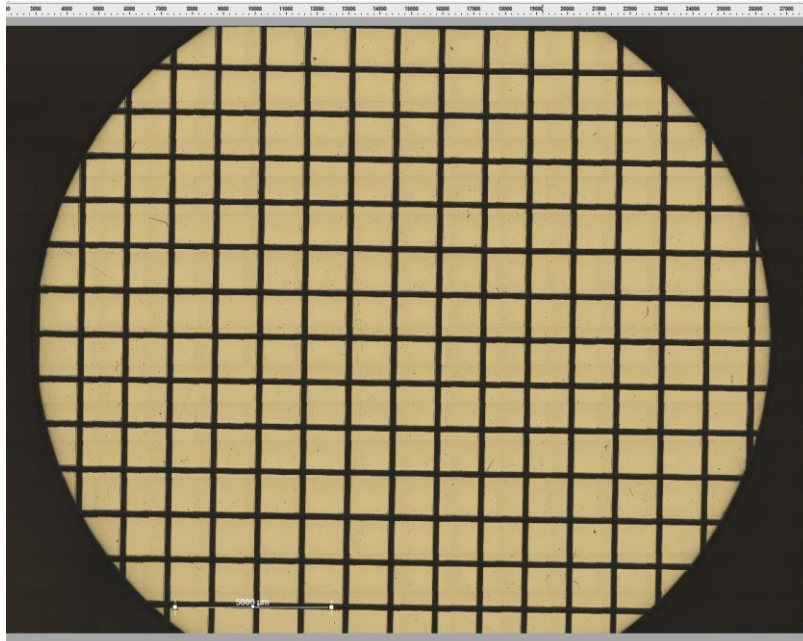


Figure 11: Image for a textured specimen

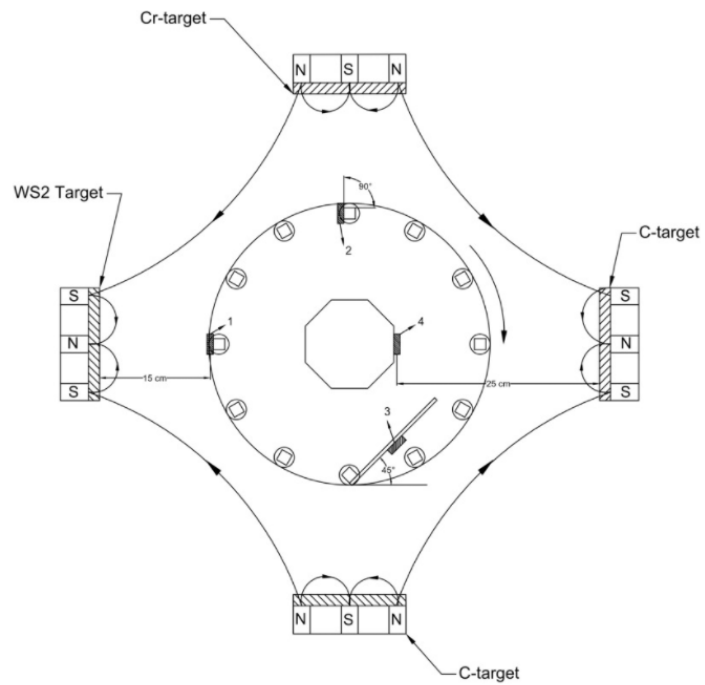


Figure 12: Top view showing the process of deposition [58]

## 3.2 Characterization Techniques

This section briefly explains the characterization techniques that are used in this project. These techniques allow the analysis of smooth and textured surfaces before and after undergoing tribological experiments. The analysis of contacting surfaces is particularly useful for studying the mechanisms involved in friction and wear for both textured and smooth surfaces. Textured surfaces were characterized after coating using 3D optical microscopy to measure textures parameters.

### 3.2.1 3D Optical Microscopy

3-D optical microscope, often referred to as a light microscope, is a type of microscope that uses visible light and a system of lenses to magnify images of small samples. The image from an optical microscope can be captured by normal light-sensitive cameras to generate a micrograph. Originally images were captured by the photographic film, but modern developments to charge-coupled devices, CCD cameras, allow the capture of digital images. Purely digital microscopes are now available what uses a CCD camera to examine a sample showing the resulting image directly on a computer screen without the need for eyepieces. The development of super-resolved fluorescence microscopy on the 8th of October 2014 brought Optical microscopy into the Nano dimension. A 3D image of the surface can be projected to a 2-D graph in order to measure both surface roughness and profile of the specimen. Texture's depth, width, and spacing can be measured afterward. Moreover, it is useful for the study of wear tracks after tribological tests are performed. Alternatives to optical microscopy, which do not use visible light, include scanning electron microscopy and transmission electron microscopy.

### 3.2.2 Scanning Electron Microscopy (SEM)

Studying surfaces at the nano level is not possible with the use of optical microscopes, due to the wavelength of light causing a resolution limit. SEM uses an electron beam that has a significantly shorter wavelength than that of a light beam allowing us to observe a structure down to several nanometers [59].

Scanning electron microscopy (SEM) scans the surface with a high-energy electron beam in a raster scan pattern and forms the image. The primary electron beam, which is produced under a high vacuum, is scanned across the surface of a specimen. The elemental composition can also be done by installing an electron dispersive spectroscopy (EDS) detector on the SEM set-up [60]. The use of SEM is useful to study the behavior of wear

debris after experimental analysis, and to check for the continuity of the WSC coating inside the grooves.

### 3.3 Characterization of Samples Surfaces

#### 3.3.1 Geometrical Characterization of Specimens

Surface analysis is essential for the critical analysis of surfaces after the tribological experiments are done. These surface analyses assist in determining the effect of various textured parameters on the final tribological performance of the specimens. In the present study, six samples were analyzed in order to minimize error due to statistical variation, and average values were taken into account. The characterization of polished samples was difficult because polished samples were highly reflective. In the present work, different methods for analysis were used, such as profilometry, optical microscope, and 3D microscopy to measure the spacing between textures (L), textures depth (d), textures width (w), and the roughness parameters  $R_a$  and  $R_q$ . The Alicona infinite focus 3D microscope was useful for obtaining geometrical information of the textures. It can take multiple images varying in both Z and XY directions; all captured images are then merged, creating a 3-D image of the surface. A lower resolution of 100nm and 50X magnification is sufficient to obtain the geometrical values. However, a higher resolution and magnification is required to obtain roughness values. Figure 13 shows a 2-D profile of a textured specimen before (a) and after (b) lapping to remove the solidified rims (bulges) on the edges of the textures.

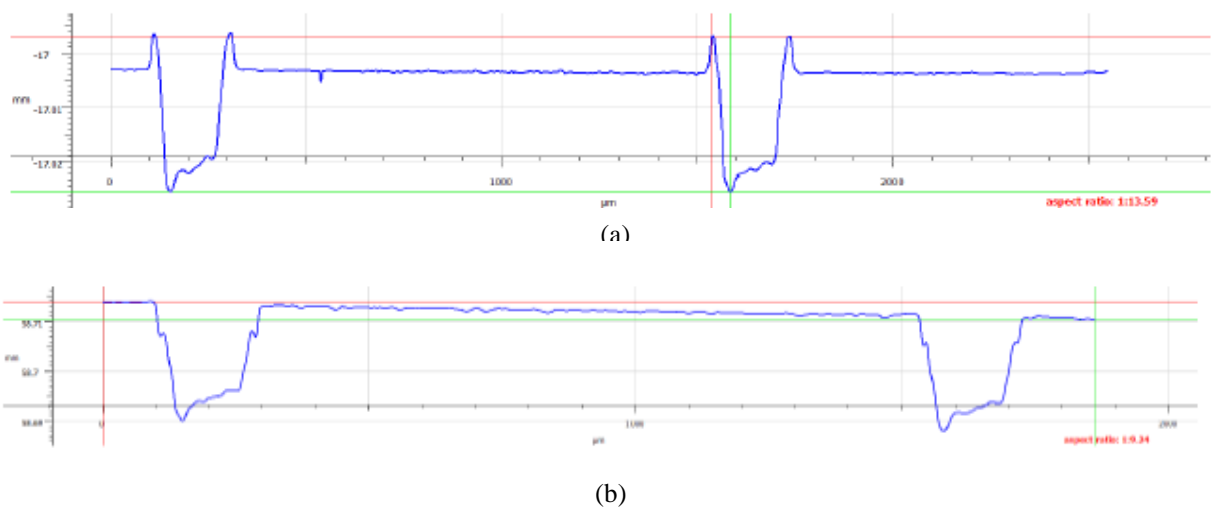


Figure 13: 2-D profile of the surface of textured specimen before and after lapping to remove the bulges at the edges

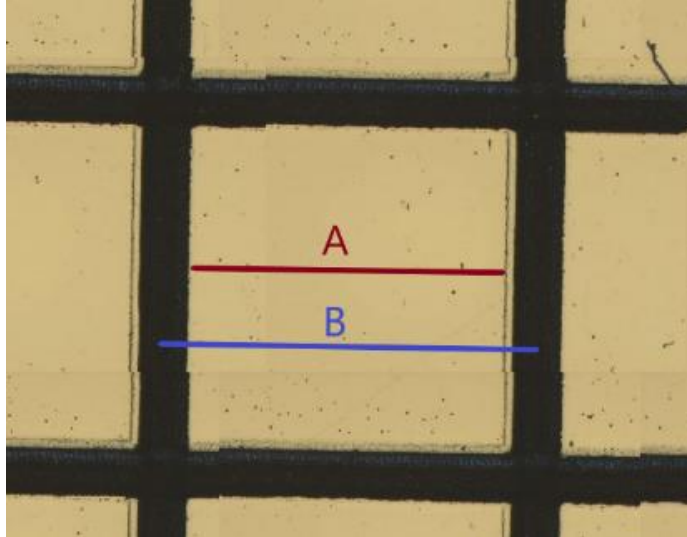


Figure 14: Texturing parameters, where A is the distance between inner edges of two adjacent grooves, and B is the distance between the centers of two adjacent grooves

Table 7 summarizes the geometrical parameters of surface textures. Textured area density calculated as  $1 - \frac{A^2}{B^2}$ .  $A = 1.25 \mu\text{m}$ ,  $B = 1.45 \mu\text{m}$ , where A and B are shown in Figure 14.

Table 7: Texturing geometrical details (averaged values)

Distance between grooves	Groove width	Groove depth	Cross-section depth	Textured area density
1.45 mm	200 $\mu\text{m}$	18 $\mu\text{m}$	36 $\mu\text{m}$	25.6%

The parameters listed in Table 7 are explained below:

- Distance between grooves: the perpendicular distance between two adjacent grooves centers
- Groove width: The width of a single groove
- Groove depth: The distance between specimens' surface and the groove's floor.
- Cross-section depth: The distance between specimens' surface and the floor of the intersection of grooves (small square). It is deeper than the normal depth of groove because the laser beam passes by these areas twice.
- Textured area density: The ratio of textured region to all specimen's surface.

### 3.3.2 Morphological Analysis of Surfaces

SEM images for TC specimens inside the grooves prove that PVD coating is continuous inside the groove. Small, oxidized particles that can be seen on the surface of uncoated specimens in Figure 15 (d) are successfully covered by applying the surface coating, as can be observed on the surface of TC specimens shown in Figure 15 (b). Wear tracks were not visible for coated specimens because wear rate is very low.

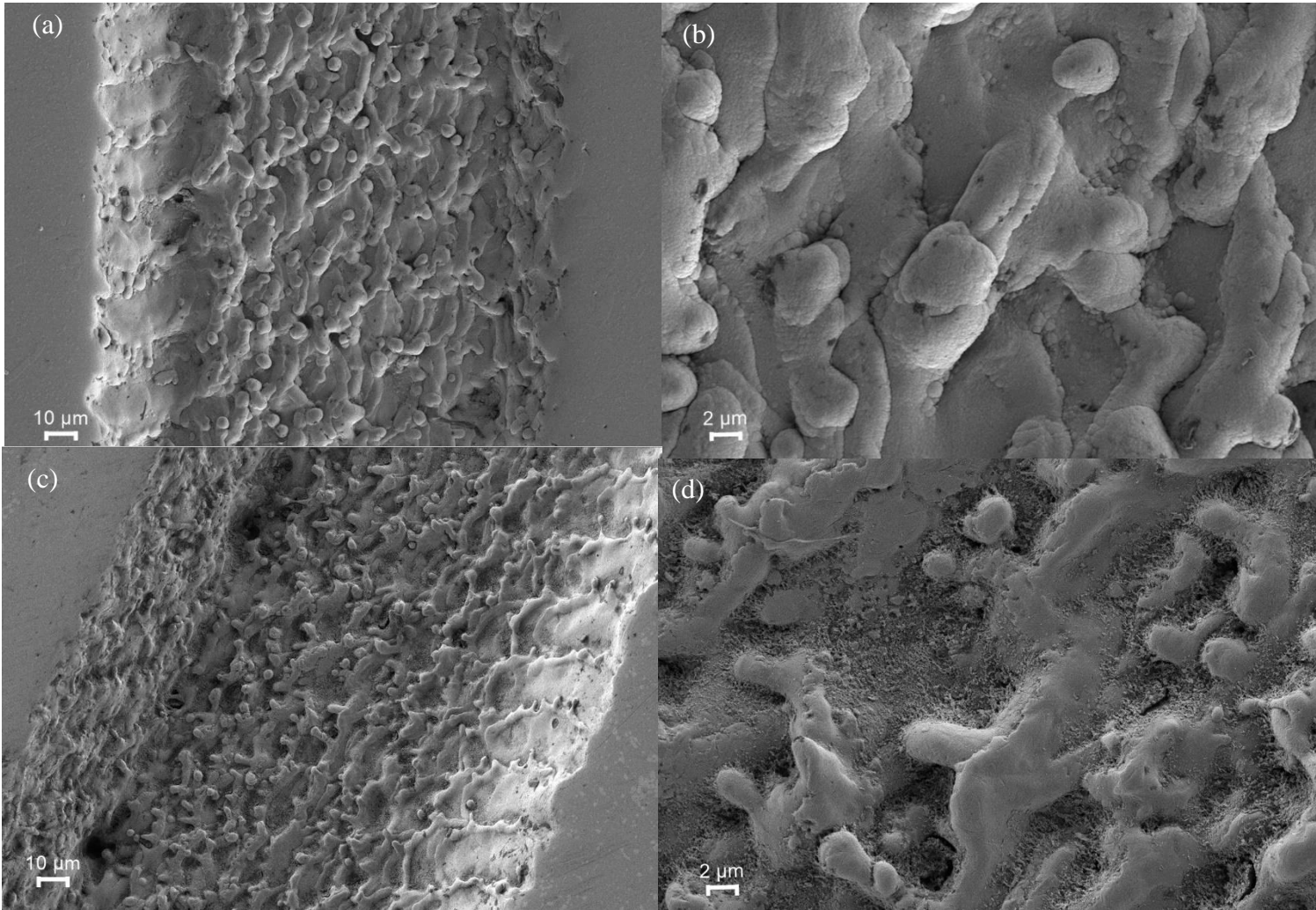


Figure 15: SEM graph for a textured specimen, after coating (a) & (b), and before coating (c) & (d)

EDS analysis for TC specimens was performed to check for the chemical composition of the surfaces for the TC specimens. EDS spots are shown in Figure 16. The following is a description for studied spots:

- TC 1.1: Outside the groove, inside the wear track
- TC 1.2: Outside the groove, outside the wear track
- TC 1.3, 2.1, and 2.2: inside the groove at different points

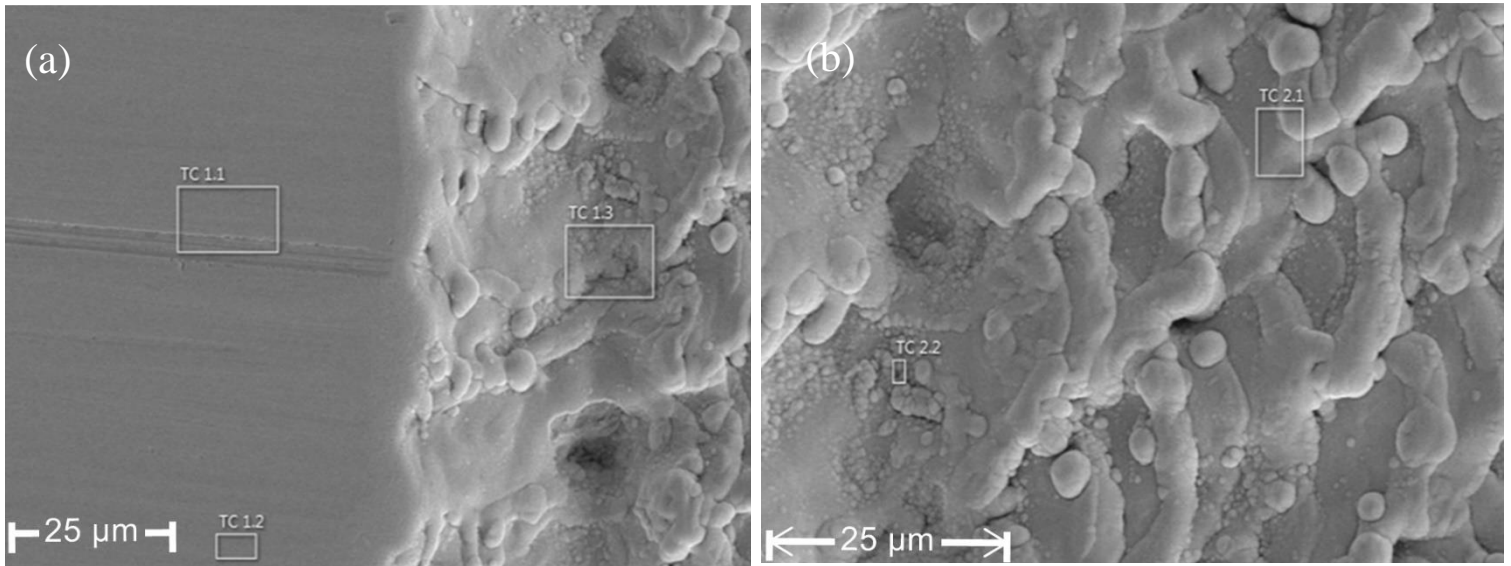


Figure 16: Spots chosen for EDS analysis on a coated textured specimen

The results of the EDS analysis are listed in Table 8. Tungsten, carbon, and sulfur are present in all analyzed spots, indicating that the coating is successfully applied inside the grooves. The presence of Argon is due to its usage as a sputtering gas. Iron was detected inside the grooves, suggesting the possibility that the coating is thinner inside the groove, causing a very small detection of iron.

Table 8: EDS results by atomic composition for a textured coated specimen at different spots

	<b>Atomic %</b>				
<b>Spectrum label</b>	Tc 1.1	Tc 1.2	Tc 1.3	Tc 2.1	Tc 2.2
<b>C</b>	64.78	65.79	68.17	65.51	60.6
<b>O</b>	2.12	1.31	3.20	2.01	3.19
<b>S</b>	19.19	19.04	17.00	18.54	19.49
<b>Ar</b>	0.57	0.61	0.42	0.46	0.35
<b>Fe</b>	-	-	0	0.18	0.13
<b>W</b>	13.34	13.26	11.21	13.3	16.24
<b>Total</b>	100	100	100	100	100

### 3.4 Tribological Experiments

Tribological experiments were carried out using a pin-on-disk machine at IPN using multifunctional tribometer MFT-5000 from RTE instruments. Experiments included the use of both flat and spherical counter-bodies using reciprocating and unidirectional sliding modules under both dry and lubricated conditions. The details of experimental parameters are listed in this section.

#### 3.4.1 Pin-on-disk

Pin-on-disk is one of the most commonly used tribological experiments for measuring friction and wear [61]. The reason behind using it is its simplicity regarding installation and set-up, while still being able to imitate a lot of tribological applications. The mechanical apparatus of this technique consists of a stationary pin (typically cylindrical or spherical shape), pressed against a rotating disk under a given load and speed, as can be observed in Figure 17. Sensors are installed to continuously measure force resistance (friction) and thermal load. A special type of transducer (load cell) converts input mechanical force into an electrical signal.

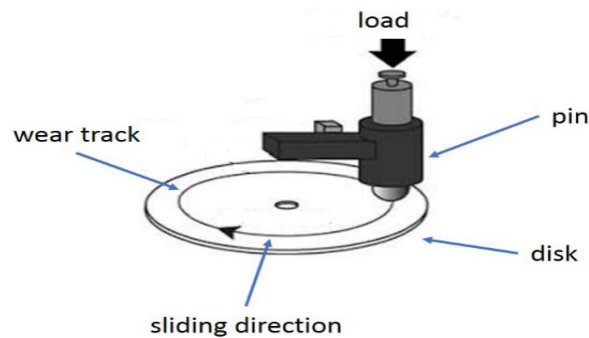


Figure 17: Schematic diagram for pin-on-disk [61]

Pin-on-disk can be performed under different lubrication conditions. For lubricated cases, the pin can be submerged in lubricant, as can be seen in Figure 18.

The following factors should be taken into account when performing pin-on-disk experiments:

- Pin shape: as discussed earlier, there are plenty of shapes for pins, most commonly cylindrical and spherical [61].
- Pin alignment: depending on the shape of the pin, misalignment can occur, causing uneven wear and friction [61].

- Pin material: contacting materials will undergo wear, changing pressure profile of the contact which will affect lift and lubrication regime, as well as having different wear mechanism [61].
- Pin location: can be either on top of the disk, or on the bottom. The location affects the results of the experiments due to wear particles getting either entrapped or leaving the contact [61].

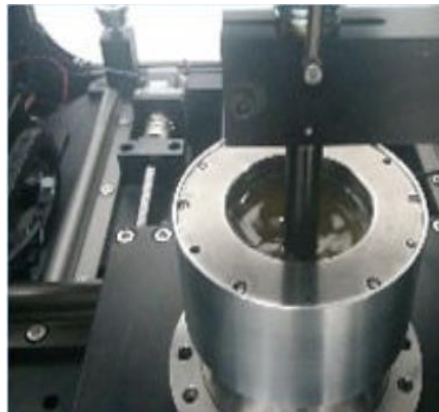


Figure 18: Submerged pin, pin on disk

In our experiments, two counter-bodies were used: a flat cylinder and a ball. Counter-body is pressed against the sample with a constant load. Normal load and friction force between sliding surfaces were continuously monitored, thus providing real-time values for COF. Continuously monitoring the normal load gives an indicator of the presence of any misalignment in the contact. The effect of surface texturing for steel (both TMD coated and not) on COF was investigated. The experimental set-up is shown in Figure 20. Each specimen was ultrasonically cleaned in a heptane bath and then dried before commencing the tests. Experiments were done at room temperature of  $22 \pm 2^\circ\text{C}$  and relative humidity of  $40 \pm 5\%$ .

Misalignment in the sample is checked before starting the experiments, as illustrated in Figure 19, to make sure that no tilting is caused by either residual lubricant or improper fixing of the specimen.



Figure 19: alignment-check tool pre-testing

For point contact, when using spherical pin, maximum contact pressure and contact area are calculated according to Hertz theory [62]. Minimum film thickness and Tallian parameter are calculated using Hamrock & Dowson equations [63]. The equations are shown below:

**Maximum contact pressure calculation:** [62]

Given that the contact is between a ball and a flat surface, it is assumed that  $R_x = R_y = R$ .

$$\frac{1}{E'} = \frac{1}{2} \left( \frac{1 - \nu_1^2}{E_1} + \frac{1 - \nu_2^2}{E_2} \right) \quad \text{(Effective Young Modulus)}$$

$$a = \sqrt[3]{\frac{3F}{8} \frac{d_1}{E'}} \quad \text{(Radius of circular area of contact for ball-plane)}$$

$$P_{max} = \frac{3F}{2\pi a^2} \quad \text{(Maximum contact pressure for ball-plane)}$$

Where:

$E_1$  is the Young modulus of the ball [Pa]

$E_2$  is the Young modulus of the test surface [Pa]

$E'$  is the effective Young modulus [Pa]

$\nu_1$  is the Poisson ratio of the ball

$\nu_2$  is the Poisson ratio of the test surface

$F$  is the normal load [N]

$d_1$  is the diameter of the ball [m]

### Minimum film thickness calculation ( $h_{min}$ ) [63]:

$$h_{min} = RH_{min}$$

$$H_{min} = \frac{3.63 U'^{0.68} G'^{0.49} (1 - e^{-0.68k})}{Q'^{0.073}}$$

$$U' = \frac{\eta U}{2E'R}$$

(Minimum film thickness)

$$G' = \lambda E'$$

$$Q' = \frac{Q}{E'R^2}$$

$$k = 1.03 \left( \frac{R_y}{R_x} \right)^{0.64}$$

Where:

$\eta$  is the dynamic oil viscosity at atmospheric pressure [ $\text{Pa s}^{-1}$ ]

$U$  is the entrance velocity of the oil into the contact [ $\text{m s}^{-1}$ ]

$R$  is the radius of the ball [m]

$\lambda$  is the pressure coefficient of viscosity [ $\text{Pa}^{-1}$ ]

$Q$  is the normal load [N]

### 3.5 Reciprocating Lubricated Pin-on-disk

Both spherical and flat pins was used with an applied constant load of 5N. sample holder reciprocates at different speeds (0.2-13 Hz) with a stroke length of 13mm, corresponding to sliding speeds of (5.2-338mm/s). Surface textures were positioned  $30^\circ$  -  $60^\circ$  relative to the direction of motion.

The lubricant was supplied from Lubrizol, ACEA E6-16, with low SABS [Sulphated Ash, Phosphorus, and Sulphur], with viscosity index  $\approx 106$ , and dynamic viscosity of 104 mPa.s at  $23^\circ \text{C}$  as measured in our laboratory, the curve is shown in Figure 21.

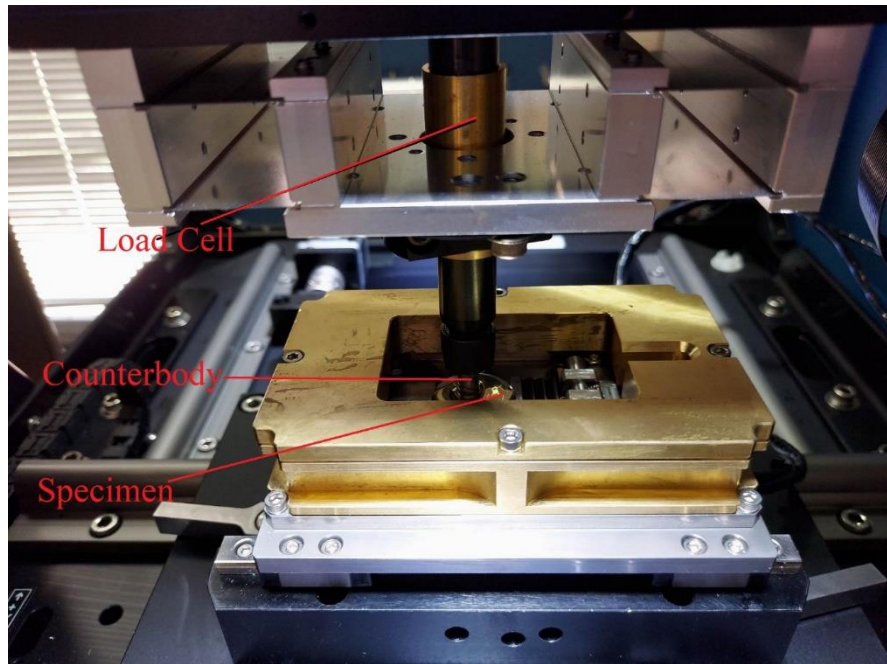


Figure 20: Experimental set-up used, reciprocating pin on disk

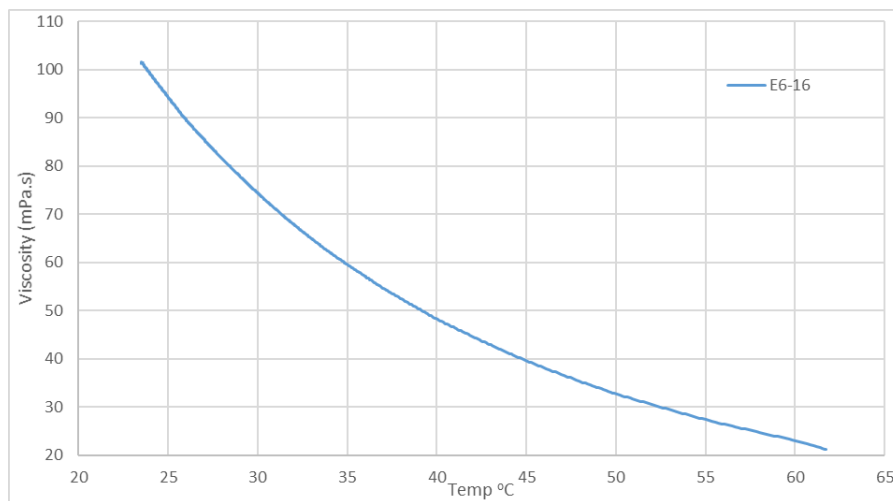


Figure 21: Viscosity curve for E6-16 lubricant

### 3.5.1 Spherical Pin

In these experiments, a ball is made of 100Cr6 steel with a radius of 5mm,  $R_a \approx 0.05\mu\text{m}$  shown in Figure 22. The calculated maximum Hertzian contact pressure is approximately 0.8 GPa, and the contact radius is 55  $\mu\text{m}$ .



Figure 22: ball used as counter-body, installed in the holder

### 3.5.2 Flat-on-Flat

For flat-on-flat contact, SAE 316L stainless steel flat pin was used. It has a shape of a cylinder with a radius of 6.35mm. The pin was polished before experiments to reduce waviness and roughness.

### 3.6 Reciprocating Dry Contact

Dry tests were done using the same spherical pin mentioned above on the reciprocating module with a constant load of 5N and 4hz – 106mm/s speed. Each test was run for 3 minutes. Each specimen was tested three times.

### 3.7 Unidirectional Lubricated Experiments

Fully formulated gear oil (ISO VG 150) was used in these experiments. The spherical pin was used with an applied constant load of 10N rotating at different speeds (up to 300RPM – 157mm/s).

## 4. Results and Discussions

The present chapter presents the outcomes of the tribological experiments of this thesis and their analysis, and the results are also discussed in this chapter. Each of the points that can be seen on any Stribeck curve in this chapter shows the averaged coefficient of friction for a minimum of three experiments performed at that speed.

### 4.1 Preliminary Results

Multiple trials were done to understand how surface texturing would affect the behavior of COF. At the beginning, a home-made modification of cylindrical counter-body to allow for line contact studies was made, as shown in Figure 23.

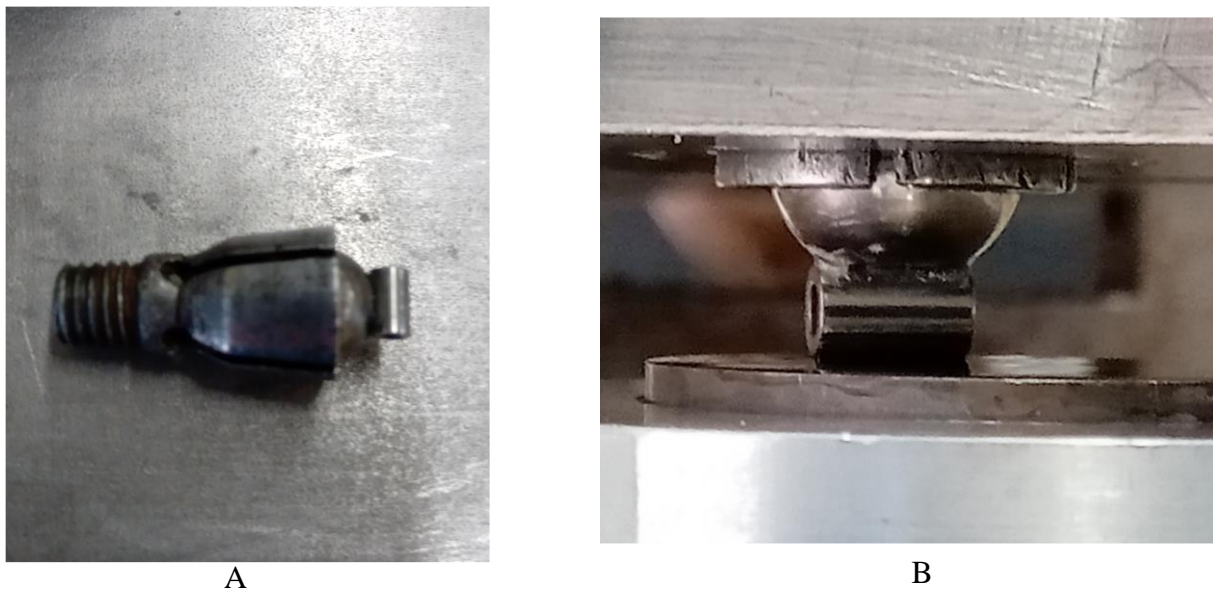


Figure 23: Home-made modification for a cylindrical counter-body. (A) is side view, (B) is the counter-body installed in the tribo-tester

This set-up resulted in highly unreliable and unrepeatable results. The main reason behind the discrepancy of the results was attributed to misalignment of the counter-body. Since the ball can rotate in all directions, it is very difficult to attain good alignment. A simple modification was made to limit the movement of the counter-body, as shown in Figure 24, where the cylinder is glued inside the counter-body holder, to attain a better alignment.

The modification shown in Figure 24 improved the repeatability, but the results were still unreliable, mainly due to residual glue lift inside the counter-body holder, causing slight misalignment. Figure 25 shows how unreliable the results were. The shift on the Stribeck curve can occur due to multiple reasons such as moving the arm or removing and installing the counter-body.

Due to the unrepeatability of the results from this tribometer, a new tribometer was used with the capabilities to perform both reciprocating and unidirectional tests, using both spherical and flat counter-body. The results of the new tribometer were repeatable and are shown in the next sections.



Figure 24: Modification to allow for a better alignment for the cylindrical counter-body. (A) is side view, (B) is the counter-body installed in the tribo-tester

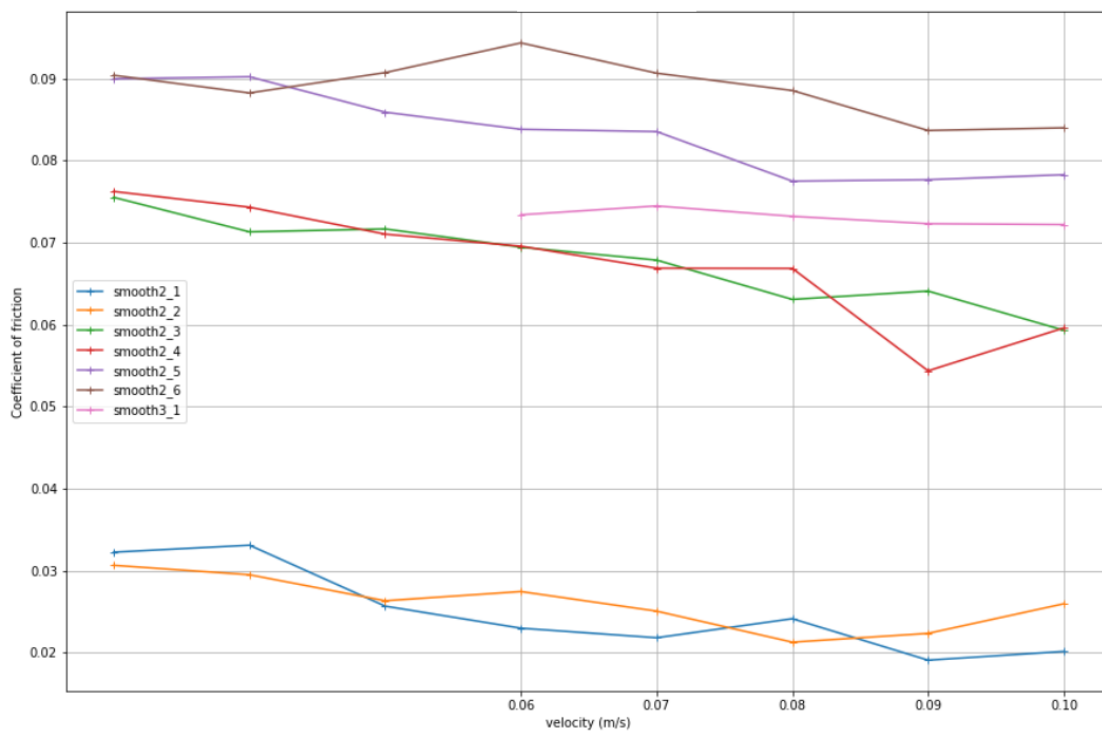


Figure 25: Results of pin-on-disk with home-made cylindrical counter-body, same specimen was tested. The tests were performed on different days, using different counter-bodies to test for repeatability.

## 4.2 Reciprocating Lubricated Pin-on-disk (ball)

Stribeck curve for textured, smooth, coated, and uncoated specimens for reciprocating tests are shown in Figure 26.

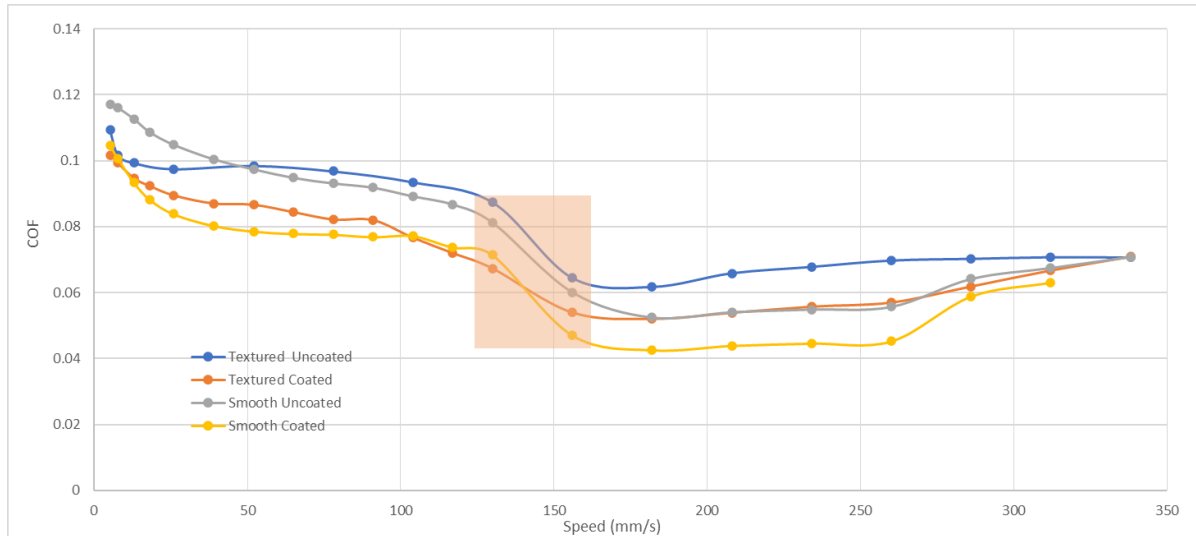


Figure 26: Stribeck curve using pin-on-disk, with spherical pin, 5N load, E6-16 lubricant, and reciprocating sliding. Comparison between textured, smooth specimens (coated and uncoated).

- For both boundary and mixed lubrication regimes two mechanisms are affecting the COF when considering textured uncoated specimens.
  - o COF reduction because surface grooves serve as a lubricant reservoir, continuously supplying lubricant to the contact [26]
  - o COF increase due to the increased surface roughness by applying surface texturing
- For uncoated specimens in boundary regime, at low speeds, grooves caused a reduction in the COF mainly due to effectively trapping lubricant and wear debris, but as the speed is increased, more pressure is generated to lubricate the contact, causing the smooth sample to perform better. These results are in agreement with both Gachot et al. [26], and Andersson et al. [53], where a COF reduction was observed in the boundary lubrication regime for textured specimens (dimples).
- For coated specimens in boundary regime, texturing was not beneficial because COF generated from asperity-to-asperity contact is low, as TMD layers are easily sheared.
- In mixed lubrication regime, textured samples caused a small increase of the COF, similarly, to results previously reported [64], [65].
- At the beginning of the hydrodynamic regime, COF for textured specimens is higher due to the reduction of pressure caused by grooves in HD contact, and therefore the

reduction of the viscosity of the lubricant which in turn, reduces the lubricant thickness [26], [65].

- At higher reciprocating speeds, more hydrodynamic pressure is generated, increasing lubricant thickness. In this region, all specimens start converging to a similar COF.

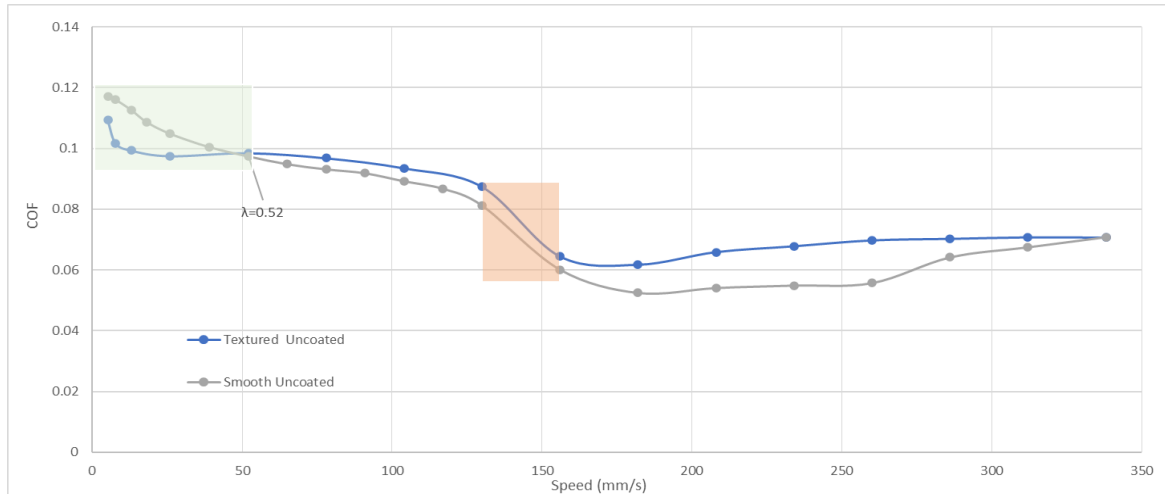


Figure 27: Stribeck curve using pin-on-disk, with spherical pin, 5N load, E6-16 lubricant, and reciprocating sliding. Comparison between textured, smooth specimens (uncoated)

### 4.3 Reciprocating Lubricated Flat-on-flat

The behavior of COF from flat-on-flat experiments is similar to what was observed earlier on pin-on-disk, as can be seen in Figure 28.

- At low speeds, from the boundary regime to the beginning of the mixed regime, textured specimens show a reduction of COF because grooves act as a lubricant reservoir [65].
- During mixed lubrication regime, smooth specimens COF starts shifting to lower values than textured specimens [65].
- Going into the HD regime, textured specimens shows higher COF because the grooves are causing pressure reduction, which in turn reduces the viscosity of the lubricant [26], [65].

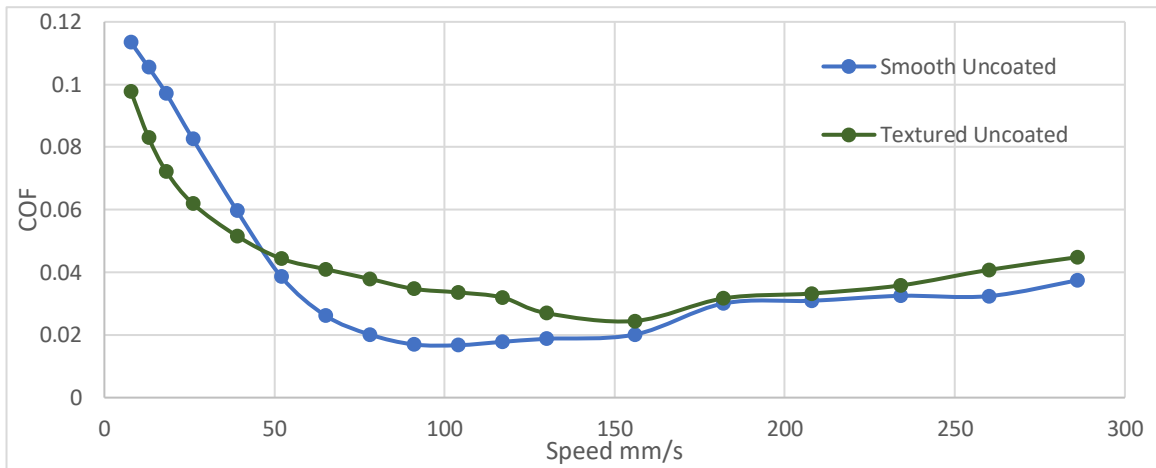


Figure 28: flat-on-flat Stribeck curve, 5N load, reciprocating module, E6-16 lubricant

#### 4.4 Unidirectional Lubricated Tests

In this test, only mixed lubrication regime is covered because the lubricant used has high viscosity, and maximum speed limited to 300RPM, corresponding to 150mm/s, trying higher speeds caused lubricant leakage that might damage the machine. Surface texturing had adverse effects while using this lubricant for both coated and uncoated specimens as can be seen on Figure 29 and Figure 30. In this section, the beneficial effect of surface texturing in BL regime was not apparent due to the fact that asperity to asperity contact was limited because the lubricant used is more viscous, as well as being rich in additives. Lubricant's additives (anti-wear) and ZDDP form a tribo-film on the surface, reducing COF. Similar results were obtained by Vilhena et al. [31] using rhombic grooves with 44% textures density

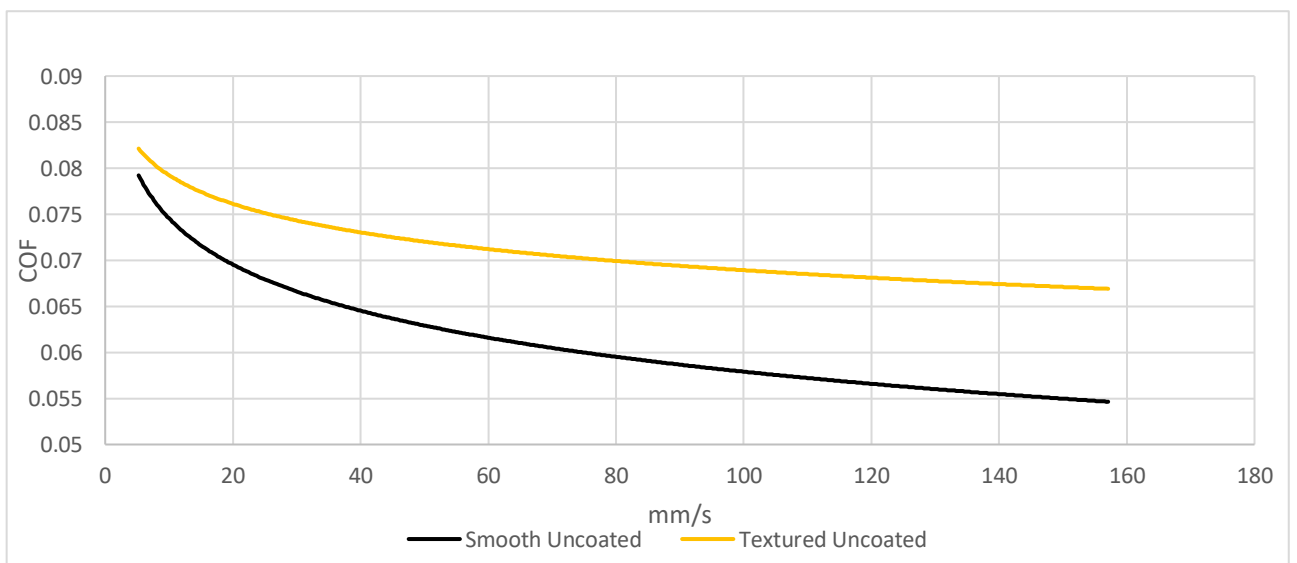


Figure 29: pin-on-disk, fully formulated ISO VG 150, 10N, unidirectional, comparison between uncoated specimens

Figure 30 compares the tribological behavior of coated specimens, smooth and textured, smooth specimens show lower COF for these testing conditions. A similar behavior can be observed from the results of flat-on-flat experiment shown on Figure 28 in the region of 50 to 100 mm/s (ML regime). We can conclude that COF for our textured specimens is always higher than smooth specimens in ML regime, regardless of the lubricant and counter body used, or sliding motion. The reason why the experiments in this section did not reach HD regime is due to instrumental limitation, limiting the maximum speed we can reach.

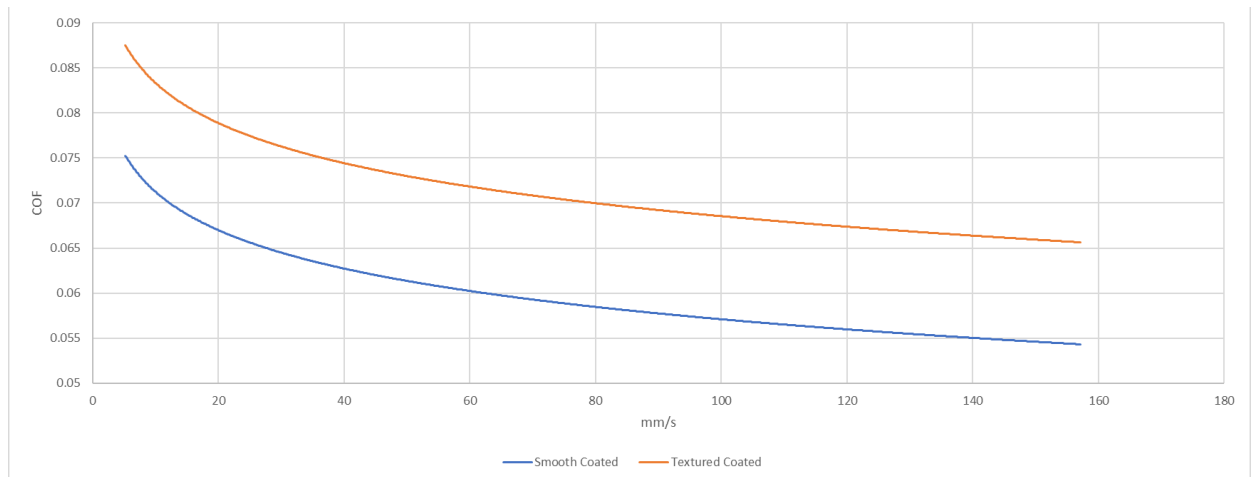


Figure 30: pin-on-disk, fully formulated ISO VG 150, 10N, unidirectional, comparison between coated specimens

#### 4.4 Reciprocating Dry Contact

Figure 31 shows COF results for the dry contact test, each specimen was tested three times, and average results presented.

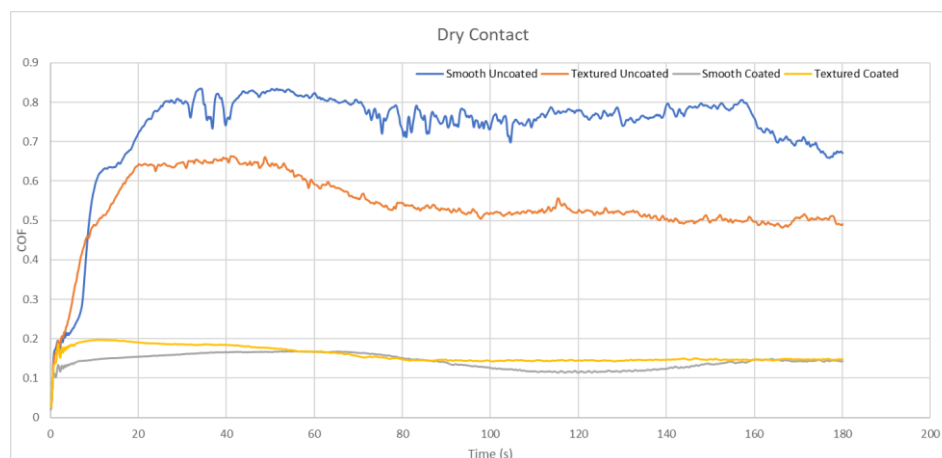


Figure 31: Dry contact COF, pin-on-disk with 5N and reciprocating module, averaged value of 3 tests.

Both coated specimens showed lower COF as expected (approx. 0.15), as W-S-C coatings serve as a solid lubricant because TMD layers are easily sheared. For uncoated specimens, surface texturing reduced the COF from 0.7 for smooth specimens to 0.5. This friction reduction is attributed to the entrapment of wear debris, reducing abrasive wear, as shown in Figure 32. For coated specimens, surface texturing did not show any effect because wear debris are soft W-S-C particles. Similar results are found by Meng et al. [41] when using

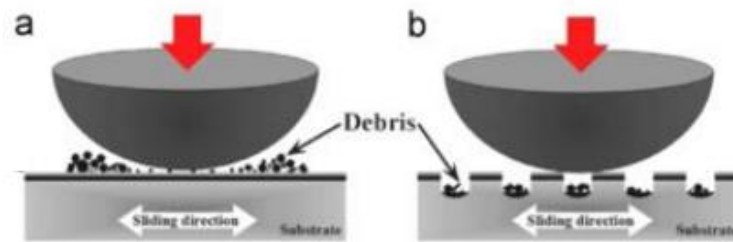


Figure 32: Wear entrapment mechanism for dry contact [66]

lines surface textures.

SEM analyses were done on wear tracks to check for wear debris inside the grooves. However, SEM graphs outside (Figure 35) and inside (Figure 34) wear tracks were similar because of two reasons:

- Textured specimens were polished to remove the bulges within the edges of the textures, causing some debris to be stuck in the grooves that are difficult to remove when cleaning the surfaces.
- Surface texturing melts specific regions on the surface to form the desired textures, causing some oxidization inside the grooves. Oxidized particles have similar physical and chemical structures to wear debris.

Wear debris observed in Figure 33 (b) are similar to oxidized particles due to LST in both Figure 35 (b) and Figure 34 (b).

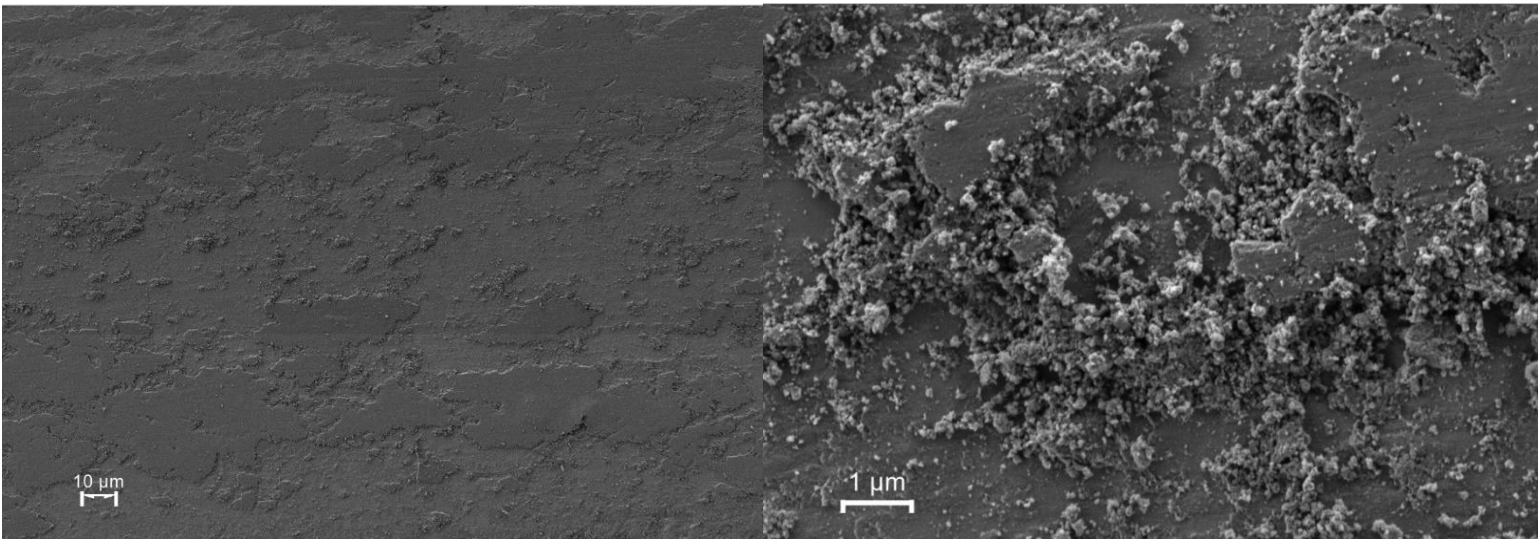


Figure 33: SEM images for untextured uncoated specimen after performing pin-on-disk dry tests with ball counter-body, inside the wear track at different magnifications.

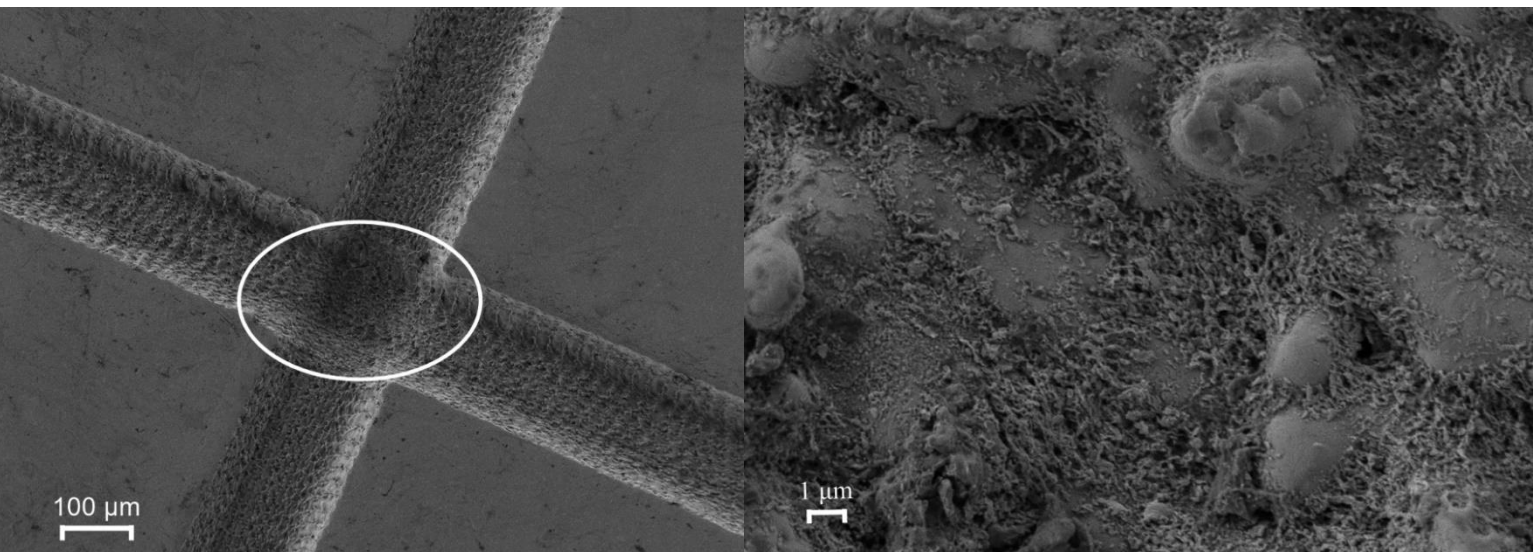


Figure 35: SEM images for the textured uncoated specimen at the intersection of two grooves, after performing pin-on-disk dry tests with ball counter-body, outside the wear track at different magnifications.

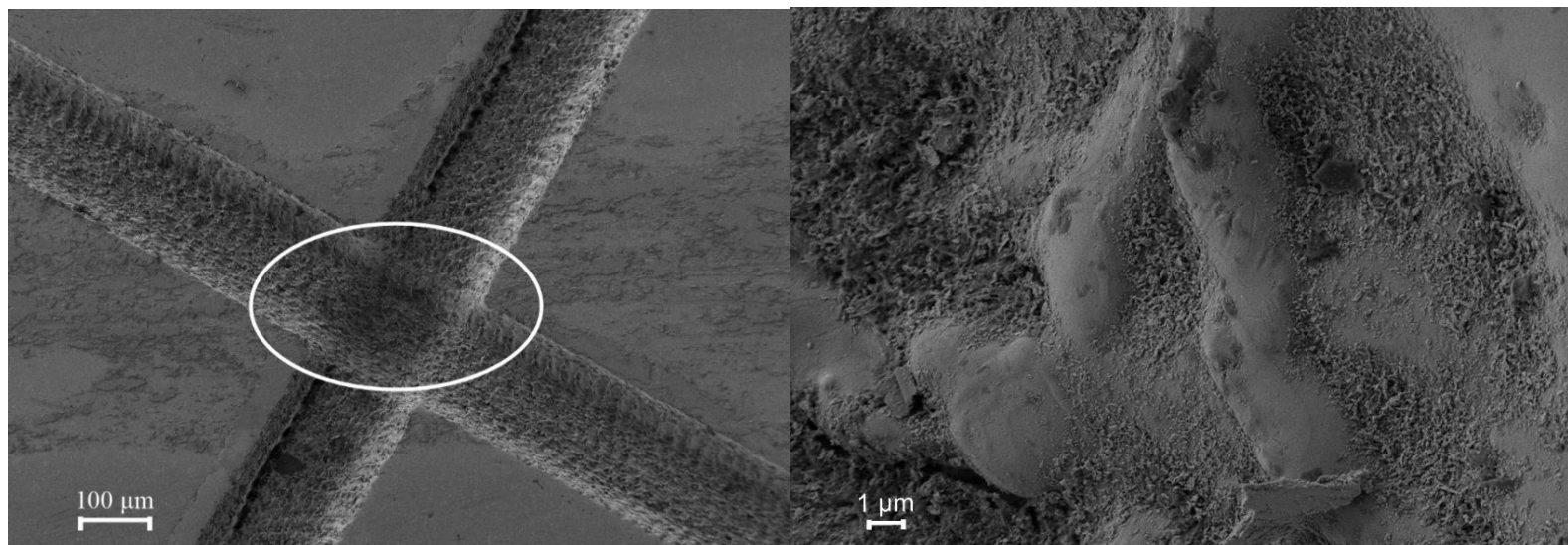


Figure 34: SEM graph for the textured uncoated specimen at the intersection of two grooves, after performing pin-on-disk dry tests with ball counter-body, inside the wear track at different magnifications.

## 5. Conclusions

### 5.1 Conclusions

- This work showed the effects of surface texturing in hydrodynamic, mixed, and boundary regimes for TMD-coated and non-coated specimens and the potential of surface texturing to reduce friction. This study focused on textured patterns of perpendicular lines. The effects of type of motion, sliding speed, and lubricant viscosity were studied on friction were studied.
- Applying TMD coatings using PVD on textured specimens appears to be effective inside the grooves (no discontinuity detected).
- As a general rule, applying TMD coatings on surface textured steels showed little to no improvement on tribological performance in relation to coated smooth specimens. However, no negative effects were observed
- In the scope of this project, smooth-coated specimens showed the best tribological behavior under all tests and for all lubrication regimes.
- The tribological behavior of textured uncoated surfaces was found to greatly depend on the dominant lubrication mode, lubricant viscosity, and the counter-body used.
- The beneficial effect of texturing was most apparent at low speeds at the initial phase of the BL regime because grooves act as a lubricant reservoir, constantly supplying the contact with lubricant, as well as entrapping wear particles.
- In mixed lubrication regime, COF appears to be always higher for textured specimens.
- At higher speeds, as HD regime is approached, COF appears to converge to the same value for all specimens, whether coated, textured, or not.
- For fully formulated higher viscosity oils (e.g., ISO VG 150) under unidirectional testing, surface texturing caused an increase of the COF for the studied lubrication regime (mixed lubrication regime). Surface coatings showed no effect under these conditions.
- For dry contact, both smooth and textured specimens with applied WSC coating exhibited similar tribological behavior, showing a huge reduction of COF, from 0.7 for uncoated and smooth specimens to 0.1. Whereas, for uncoated specimens, surface texturing caused friction reduction from 0.7 to 0.5.
- Wear rate was negligible at all lubricated experiments.

## 5.2 Final Discussion and Recommendations

The performance of textured specimens showed that the optimum parameters are highly dependent on testing conditions. For instance, coated specimens which showed improved performance on reciprocating ball-on-disk experiments, exhibited no effect on the unidirectional module.

Finding the optimum parameters of textured surfaces that are able to outperform a smooth sample in all conditions is a rather challenging task. Each texturing shape, width, and depth have different behavior under each lubrication regime, type of contact, and lubricant used.

The performance of TMD coated and textured specimens varied depending on the type of experiments used; deeper analysis and further studies are required to pinpoint the potential of combining both textures and coatings.

For future work, it is recommended to optimize texturing parameters and perform tribological experiments with controlling lubricant viscosity (could be done by varying the temperature) to find a connection between tribological performance, texturing parameters lubricant viscosity, lubrication regime, and TMD coatings.

Due to instrumental limitations, sliding speeds higher than 300mm/s could not be achieved. It would be interesting to study the tribological behavior of perpendicular surface grooves at higher sliding speeds than the ones tested in this thesis. It would also be interesting to investigate different types of contact, e.g., block-on-ring, to study the behavior of TMD-coated perpendicular surface textures. Studying the wear behavior for textured and untextured specimens in dry contact tests could prove to be beneficial.

## Bibliography

- [1] Nakada M. Trends in engine technology and tribology. *Tribology International*. 1994 Feb 1;27(1):3-8.
- [2] Rudnick LR, editor. *Lubricant additives: chemistry and applications*. CRC press; 2017 Jul 12.
- [3] Neville A, Morina A, Haque T, Voong M. Compatibility between tribological surfaces and lubricant additives—how friction and wear reduction can be controlled by surface/lube synergies. *Tribology international*. 2007 Oct 1;40(10-12):1680-95.
- [4] Hamilton, D. B., J. A. Walowit, C. M. Allen. A theory of lubrication by microirregularities. 1966 Mar;88:177-185.
- [5] Anno, James N., J. A. Walowit, C. M. Allen. Microasperity lubrication. 1968 351-355.
- [6] Willis E. Surface finish in relation to cylinder liners. *Wear*. 1986 May 1;109(1-4):351-66.
- [7] Wakuda M, Yamauchi Y, Kanzaki S, Yasuda Y. Effect of surface texturing on friction reduction between ceramic and steel materials under lubricated sliding contact. *Wear*. 2003 Feb 1;254(3-4):356-63.
- [8] Wang X, Kato K, Adachi K, Aizawa K. Loads carrying capacity map for the surface texture design of SiC thrust bearing sliding in water. *Tribology international*. 2003 Mar 1;36(3):189-97.
- [9] Etsion I, Kligerman Y, Halperin G. Analytical and experimental investigation of laser-textured mechanical seal faces. *Tribology Transactions*. 1999 Jan 1;42(3):511-6.
- [10] Yu XQ, He S, Cai RL. Frictional characteristics of mechanical seals with a laser-textured seal face. *Journal of Materials Processing Technology*. 2002 Oct 11;129(1-3):463-6.
- [11] Tung SC, McMillan ML. Automotive tribology overview of current advances and challenges for the future. *Tribology International*. 2004 Jul 1;37(7):517-36.
- [12] Baumgart P, Krajnovich DJ, Nguyen TA, Tam AG. A new laser texturing technique for high performance magnetic disk drives. *IEEE Transactions on Magnetics*. 1995 Nov;31(6):2946-51.
- [13] "mold-technology4all," 20 08 2011. [Online]. Available: <http://mold-technology4all.blogspot.com/>. [Accessed 20 01 2021].

- [14] Geiger M, Popp U, Engel U. Excimer laser micro texturing of cold forging tool surfaces-influence on tool life. *CIRP Annals*. 2002 Jan 1;51(1):231-4.
- [15] Geiger M, Roth S, Becker W. Influence of laser-produced microstructures on the tribological behaviour of ceramics. *Surface and Coatings Technology*. 1998 Mar 1;100:17-22.
- [16] Patel D, Jain VK, Ramkumar J. Micro texturing on metallic surfaces: State of the art. *Proceedings of the Institution of Mechanical Engineers, Part B: Journal of Engineering Manufacture*. 2018 May;232(6):941-64.
- [17] Guo AN, Wang XJ, Gang S, Jiang DF. Numerical analysis of annular seal with different distribution of surface texture. In *Key Engineering Materials 2015* 642:66-71.
- [18] Martz LS. Preliminary report of developments in interrupted surface finishes. *Proceedings of the Institution of Mechanical Engineers*. 1949 Jun;161(1):1-9.
- [19] Spencer, Andrew. Optimizing surface texture for combustion engine cylinder liners. Diss. Luleå tekniska universitet, 2010.
- [20] Schmid J. Large engine cylinder honing as a contribution to emissions reduction. *MTZ industrial*. 2013 May 1;3(1):48-53.
- [21] Ike H. Nanoscopic surface texture formed by indentation and sliding of a smooth wedge tool. *Wear*. 2005 Apr 1;258(9):1404-10.
- [22] Costa HL, Hutchings IM. Effects of die surface patterning on lubrication in strip drawing. *Journal of Materials Processing Technology*. 2009 Feb 1;209(3):1175-80.
- [23] Li, Yufeng, Aric K. Menon. The development and implementation of discrete texture for the improvement of tribological performance. 1995;279-284.
- [24] Muecklich F, Lasagni A, Daniel C. Laser Interference Metallurgy—using interference as a tool for micro/nano structuring. *Zeitschrift für Metallkunde*. 2006;97(10):1337-44.
- [25] Gachot C, Catrin R, Lasagni A, Schmid U, Mücklich F. Comparative study of grain sizes and orientation in microstructured Au, Pt and W thin films designed by laser interference metallurgy. *Applied Surface Science*. 2009 Mar 1;255(10):5626-32.
- [26] Gachot C, Rosenkranz A, Hsu SM, Costa HL. A critical assessment of surface texturing for friction and wear improvement. *Wear*. 2017 Feb 15;372:21-41.
- [27] Hsu SM. *Surface texturing: principles and design*. National Institute of Standards & Technology: Gaithersburg, MD, USA. 2006 Nov 6.
- [28] Siripuram RB, Stephens LS. Effect of deterministic asperity geometry on hydrodynamic lubrication. *J. Trib..* 2004 Jul 1;126(3):527-34.

- [29] Pettersson U, Jacobson S. Friction and wear properties of micro textured DLC coated surfaces in boundary lubricated sliding. *Tribology letters*. 2004 Oct 1;17(3):553-9.
- [30] Rashwan, Ola, *Micro Surface Texturing for Friction Control*. Electronic Theses and Dissertations. 2013.
- [31] Vilhena LM, Ramalho A, Cavaleiro A. Grooved surface texturing by electrical discharge machining (EDM) under different lubrication regimes. *Lubrication Science*. 2017 Nov;29(7):493-501.
- [32] Sung SH, Schnitzer N, Brown L, Park J, Hovden R. Stacking, strain, and twist in 2D materials quantified by 3D electron diffraction. *Physical Review Materials*. 2019 Jun 25;3(6):064003.
- [33] Polcar T, Gustavsson F, Thersleff T, Jacobson S, Cavaleiro A. Complex frictional analysis of self-lubricant WSC/Cr coating. *Faraday Discussions*. 2012;156(1):383-401.
- [34] Lansdown AR. *Molybdenum disulphide lubrication*. Elsevier; 1999 May 28.
- [35] Kubart T, Polcar T, Kopecký L, Novak R, Novakova D. Temperature dependence of tribological properties of MoS<sub>2</sub> and MoSe<sub>2</sub> coatings. *Surface and Coatings Technology*. 2005 Apr 1;193(1-3):230-3.
- [36] Teer DG. New solid lubricant coatings. *Wear*. 2001 Oct 1;251(1-12):1068-74.
- [37] Scharf TW, Rajendran A, Banerjee R, Sequeda F. Growth, structure and friction behavior of titanium doped tungsten disulphide (Ti-WS<sub>2</sub>) nanocomposite thin films. *Thin Solid Films*. 2009 Aug 3;517(19):5666-75.
- [38] Juhasz JA, Best SM. Surface modification of biomaterials by calcium phosphate deposition. In *Surface modification of biomaterials 2011* Jan 1 (pp. 143-169). Woodhead Publishing.
- [39] Voevodin AA, O'Neill JP, Zabinski JS. Nanocomposite tribological coatings for aerospace applications. *Surface and Coatings Technology*. 1999 Sep 1;116:36-45.
- [40] Nossa A, Cavaleiro A. Chemical and physical characterization of C (N)-doped W-S sputtered films. *Journal of materials research*. 2004 Aug;19(8):2356-65.
- [41] Meng R, Deng J, Liu Y, Duan R, Zhang G. Improving tribological performance of cemented carbides by combining laser surface texturing and WSC solid lubricant coating. *International Journal of Refractory Metals and Hard Materials*. 2018 Apr 1;72:163-71.
- [42] Tønder K, Christensen H. Waviness and roughness in hydrodynamic lubrication. *Proceedings of the Institution of Mechanical Engineers*. 1972 Jun;186(1):807-12.

- [43] Spikes, H. A. (1997). Mixed lubrication—an overview. *Lubrication Science*, 9(3), 221-253.
- [44] Olver AV, Guangteng G, Spikes HA. Film thickness and pressure in micro-EHD contacts. *Tribology Series*. Vol. 38. Elsevier, 2000. 503-510.
- [45] Choo JW, Glovnea RP, Olver AV, Spikes HA. The effects of three-dimensional model surface roughness features on lubricant film thickness in EHL contacts. *Trib.* 2003 Jul 1;125(3):533-42.
- [46] Kovalchenko A, Ajayi O, Erdemir A, Fenske G, Etsion I. The effect of laser texturing of steel surfaces and speed-load parameters on the transition of lubrication regime from boundary to hydrodynamic. *Tribology Transactions*. 2004 Apr 1;47(2):299-307.
- [47] Amanov A, Cho IS, Pyoun YS, Lee CS, Park IG. Micro-dimpled surface by ultrasonic nanocrystal surface modification and its tribological effects. *Wear*. 2012 May 15;286:136-44.
- [48] Rapoport L, Moshkovich A, Perfilyev V, Lapsker I, Halperin G, Itovich Y, Etsion I. Friction and wear of MoS<sub>2</sub> films on laser textured steel surfaces. *Surface and Coatings Technology*. 2008 Apr 15;202(14):3332-40.
- [49] Borghi A, Gualtieri E, Marchetto D, Moretti L, Valeri S. Tribological effects of surface texturing on nitriding steel for high-performance engine applications. *Wear*. 2008 Sep 20;265(7-8):1046-51.
- [50] Braun D, Greiner C, Schneider J, Gumbsch P. Efficiency of laser surface texturing in the reduction of friction under mixed lubrication. *Tribology international*. 2014 Sep 1;77:142-7.
- [51] Scaraggi M, Mezzapesa FP, Carbone G, Ancona A, Tricarico L. Friction properties of lubricated laser-microtextured-surfaces: an experimental study from boundary-to hydrodynamic-lubrication. *Tribology Letters*. 2013 Jan 1;49(1):117-25.
- [52] Tian T, Wong VW. Modeling the lubrication, dynamics, and effects of piston dynamic tilt of twin-land oil control rings in internal combustion engines. *J. Eng. Gas Turbines Power*. 2000 Jan 1;122(1):119-29.
- [53] Gao L, de Boer G, Hewson R. The role of micro-cavitation on EHL: A study using a multiscale mass conserving approach. *Tribology International*. 2015 Oct 1;90:324-31.
- [54] Andersson P, Koskinen J, Varjus SE, Gerbig Y, Haefke H, Georgiou S, Zhmud B, Buss W. Microlubrication effect by laser-textured steel surfaces. *Wear*. 2007 Feb 4;262(3-4):369-79.
- [55] Xing Y, Deng J, Feng X, Yu S. Effect of laser surface texturing on Si<sub>3</sub>N<sub>4</sub>/TiC ceramic sliding against steel under dry friction. *Materials & Design (1980-2015)*. 2013 Dec 1;52:234-45.

- [56] Kang M, Park YM, Kim BH, Seo YH. Micro-and nanoscale surface texturing effects on surface friction. *Applied Surface Science*. 2015 Aug 1;345:344-8.
- [57] Wang Z, Zhao Q, Wang C, Zhang Y. Modulation of dry tribological property of stainless steel by femtosecond laser surface texturing. *Applied Physics A*. 2015 Jun 1;119(3):1155-63.
- [58] Vuchkov T, Evaristo M, Yaqub TB, Cavaleiro A. The effect of substrate location on the composition, microstructure and mechano-tribological properties of WSC coatings deposited by magnetron sputtering. *Surface and Coatings Technology*. 2020 Mar 25;386:12548.
- [59] Vernon-Parry KD. Scanning electron microscopy: an introduction. *III-Vs Review*. 2000 Jul 1;13(4):40-4.
- [60] Yan Y. Tribology and tribo-corrosion testing and analysis of metallic biomaterials. *InMetals for Biomedical Devices 2010* Jan 1 (pp. 178-201). Woodhead Publishing.
- [61] 1 7 "Tribonet," 1 7 2021. [Online]. Available: [tribonet.org](http://tribonet.org). [Accessed 1 7 2021].
- [62] Willis JR. Hertzian contact of anisotropic bodies. *Journal of the Mechanics and Physics of Solids*. 1966 May 1;14(3):163-76.
- [63] Hamrock, Bernard J, Duncan Dowson. Isothermal elastohydrodynamic lubrication of point contacts: part III—fully flooded results. 1977: 264-275.
- [64] Costa HL, Hutchings IM. Hydrodynamic lubrication of textured steel surfaces under reciprocating sliding conditions. *Tribology International*. 2007 Aug 1;40(8):1227-38.
- [65] Vladescu SC, Olver AV, Pegg IG, Reddyhoff T. The effects of surface texture in reciprocating contacts—an experimental study. *Tribology International*. 2015 Feb 1;82:28-42.
- [66] He D, Zheng S, Pu J, Zhang G, Hu L. Improving tribological properties of titanium alloys by combining laser surface texturing and diamond-like carbon film. *Tribology international*. 2015 Feb 1;82:20-7.
- [67] Bunaciu AA, Udriștioiu EG, Aboul-Enein HY. X-ray diffraction: instrumentation and applications. *Critical reviews in analytical chemistry*. 2015 Oct 2;45(4):289-99.